CHATER ONE

Introduction and Basic Concepts

1.1 Introduction

A laser is an oscillator that operates at optical frequencies. These frequencies of operation lie within a spectral region that extends from the very far infrared to the vacuum ultraviolet (VUV) or soft x - ray region (Colin E. Webb and Julian D.C. Jones 2004). The basic laser structure consists of an active optical gain medium that amplifies electromagnetic waves, a pumping source that pumps energy into the active medium, and an optical resonator that is composed of two highly reflective mirrors. The pump source could be a flash lamp, a gas discharge, or an electrical current source (Costas P. Grigoropoulos 2009). Laser light has properties that distinguish it from ordinary light. These properties are as follows:

The wavelength (color) of laser light is extremely pure (monochromatic) when compared to other sources of light,

1- All of the photons (energy) that make up the laser beam have a fixed phase relationship (coherence) with respect to one another.
2- Light from a laser typically has very low divergence. It can travel over great distances or can be focused to a very small spot with a brightness which exceeds that of the sun. Because of these properties, lasers are used in a wide variety of applications in all walks of life.
3- A laser differs from other sources of light in that it emits light coherently. Spatial coherence allows a laser to be focused to a tight spot, enabling applications such as laser micromachining, which include trimming of resistors, laser direct write, laser marking, laser annealing of semiconductors materials etc.

Laser annealing of ion-implantation damage in semiconductors devices, leads to improvement of surface structure and electrical characteristics of semiconductor. Laser annealing of silicon diodes is discussed in detail in chapter four of this thesis.

1.2 The study objectives

The objective of this study is to treat the defects of silicon diode, appear after conventional annealing, by using two infrared lasers: Q-switched Nd:YAG laser and CO_2 laser in order to enhance the characteristics and dynamic resistance of silicon diode.

1.3 Thesis structure

The basic concepts of lasers, laser properties and laser industrial applications are described in the first chapter of this thesis. Chapter two covered the applications of laser in electronics, basics of laser annealing and literature review of annealing of electronics devices. In Chapter three, a detailed description of the experimental work, the laser used in this study for treatment of samples, in addition to the instruments that were used to investigate the samples, are discussed. Then Chapter four deals with the results of the interaction of laser light with semiconductors. Defects in silicon diodes and their relationship to laser radiation are explained and discussed. At the end of this chapter, conclusions and future work are presented.

1.4 Laser industrial applications

Lasers are employed across the manufacturing industry as tools capable of delivering intense cutting or welding power with high precision. Their ability to manipulate and transform materials makes them ideal for the automobile, computer and clothing industries – to name but a few. In fact, it is difficult to

find a modern consumer product that has not seen a laser during its manufacturing.

1.4.1 Laser cutting

Most laser cutting is carried out using CO_2 or Nd:YAG lasers. The general principles of cutting are similar for both types of laser although CO_2 lasers dominate the market.

The basic mechanism of laser cutting is extremely simple and can be summarized as follows:

1. A high intensity beam of infrared light is generated by a laser.
2. This beam is focused onto the surface of the workpiece by means of a lens.
3. The focused beam heats the material and establishes a very localized melt (generally smaller than 0.5mm diameter) throughout the depth of the sheet.
4. The molten material is ejected from the area by pressurized gas jet acting coaxially with the laser beam as shown in figure 1.1. (With certain materials this gas jet can accelerate the cutting process by doing chemical as well as physical work). For example, Carbon or mild steels are generally cut in a jet of pure oxygen. The oxidation process initiated by the laser heating generates its own heat and this greatly adds to the efficiency of the process.
5. This localized area of material removal is moved across the surface of the sheet thus generating a cut. Movement is achieved by manipulation of the focused laser spot (by CNC mirrors) or by mechanically moving the sheet on a CNC X-Y table. 'Hybrid' systems are also available where the material is moved in one axis and the laser spot moved in the other. Fully robotic systems are available for profiling three dimensional shapes. Nd:YAG lasers can utilize optical fibres rather than mirrors but this option is not available for the longer wavelength CO_2 laser.

Before moving on to a more detailed description of the cutting process, now is a good time to summarize the benefits of laser cutting.

A. The process cuts at high speed compared to other profiling methods. For example a 1500W CO_2 laser will cut 2mm thick mild steel at 7.5 mm in^{-1}. The same machine will cut 5mm thick acrylic sheet at ~12mm in^{-1}.

B. In most cases (e.g. the two examples given above) the cut components will be ready for service immediately after cutting without any subsequent cleaning operation.

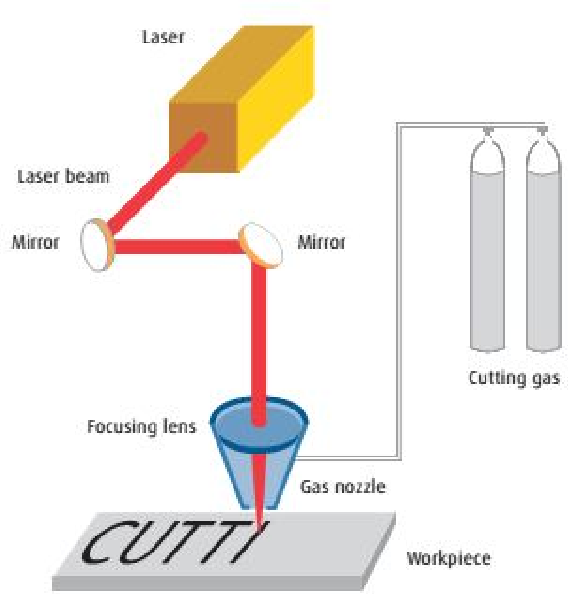

Figure 1.1 A schematic of laser cutting. The lens mount or the nozzle (or both) can be adjusted from left to right or into and out of the plane of the sketch. This allows for centralisation of the focused beam with the nozzle. The vertical distance between the nozzle and the lens can also be adjusted.

C. The cut width (kerf width) is extremely narrow (typically 0.1 to 1.0mm). Very detailed work can be carried out without the restrictions of a minimum internal radius imposed by milling machines and similar mechanical methods.

D. The process can be fully CNC controlled. This, combined with the lack of necessity for complex jigging arrangements, means that, a change of job from cutting component 'A' out of steel to cutting component 'B' out of polymer can be carried out in seconds. (Note Nd:YAG lasers cannot cut most plastics because they are transparent to Nd:YAG laser light).

E. Although laser cutting is a thermal process, the actual area heated by the laser is very small and most of this heated material is removed during cutting. Thus, the thermal input to the bulk of the material is very low, heat affected zones are minimized and thermal distortion is generally avoided.

F. It is a non-contact process, which means that material needs only to be lightly clamped or merely positioned under the beam. Flexible or flimsy materials can be cut with great precision and do not distort during cutting, as they would when cut by mechanical methods.

G. Owing to the CNC nature of the process, the narrowness of the keft width and the lack of mechanical force on the sheet being cut, components can be arranged to 'nest' very close together. Hence, material waste can be reduced to a minimum. In some cases this principle can be extended until there is no waste material at all between similar edges of adjacent components.

H. Although the capital cost of a laser-cutting machine is substantial, the running costs are generally low. Many industrial cases exist where a large installation has paid for itself in under a year.

I. The process is extremely quiet compared to competing techniques, a factor which improves the working environment and the efficiency or the operating staff.

J. Laser cutting machines are extremely safe to use in comparison with many of their mechanical counterparts (J. Powell and A. Kaplan 2004).

1.4.1.1 A comparison of CO_2 and Nd:YAG laser cutting.

CO_2 and Nd:YAG lasers both generate high intensity beams of infrared light which can be focused and used for cutting. Far fewer Nd:YAG lasers are sold as cutting machines compared with CO_2 lasers. This is because for general cutting applications, CO_2 lasers are most effective. Nd:YAG lasers are only preferred:

A. If very fine detailed work is required in thin section material.

B. If highly reflective materials such as copper or silver alloys are to be cut on a regular basis.

C. If an optical fibre is to be used to transport the laser beam to the work piece.

Although both CO_2 and Nd:YAG lasers generate infrared light, the wavelength of the CO_2 laser light is ten times that of the Nd:YAG machines (10.6 microns and 1.06 microns respectively). Because the Nd:YAG laser light has a shorter wavelength it has three advantages over CO_2 laser light:

1. Nd:YAG laser light can be focused down to a smaller spot than CO_2 laser light. This means that finer, more detailed work can be achieved (e.g. ornamental clock hands).
2. Nd:YAG laser light is less easily reflected by metal surfaces. For this reason Nd:YAG lasers are suited to work on highly reflective metals such as silver.
3. Nd:YAG light can travel through glass (CO_2 light cannot). This means that high quality glass lenses can be used to focus the beam down to a minimum spot size. Also, quartz optical fibres can be employed to carry the beam relatively long distances to the workpiece. This has led to the widespread use of Nd:YAG lasers on automobile production lines where available space on the lines is at a premium (J. Powell and A. Kaplan 2004).

1.4.2 Laser drilling

The aim in laser drilling is to get the radiant power to the bottom of a growing pit. At the bottom of the pit the radiation is absorbed and reflected. It causes the material to boil and the vapor thus produced exits from the hole with a considerable velocity (near sonic speeds) scouring the melt from the edges of the hole. Unfortunately, the vapor is also very hot and may even be plasma; it will certainly have steep thermal gradients and pressure gradients within it. There will also be considerable dust in the form of nano particles. All these effects disrupt the in-coming beam by scattering and absorbing it. For the shorter wavelengths, e.g. from Nd:YAG lasers at 1.06 µm, the absorption is small compared to the scattering effects; it is the opposite for the longer CO_2 radiation at 10.6 µm. Even shorter wavelengths are being used, for example

some excellent results have been reported using copper vapor laser operating at 510.6 or 578.2 nm. Thus one objective has been to fire the laser beam into the hole before the vapor can form and disturb the focus. Pulsed laser drilling is the result. Some sophisticated studies on the importance of pulse shaping having been written – short sharp pulses with a brief tail appears to give good debris clearance from the hole. The clearance of droplets and debris from the hole is an intermittent process. The process of laser drilling is similar to piercing prior to cutting. The intensity of a medium power focused laser beam is sufficient to raise the temperature of the material to its boiling point within picoseconds or two. For example, Table 1.1 lists the time taken to heat different materials to their boiling point for a focused 2 kW laser pulse. The amount of material removed once boiling starts is dependent on the overall energy of the pulse.

The shorter the pulse, the less conduction and the truer becomes the heat balance between the delivered energy and the material removed:

$$v = \frac{F_0}{\{\rho[L + C_p(T_v - T_0)]\}} \dots\dots\dots\dots\dots\dots\dots\dots (1-1)$$

Where v = penetration velocity m/s; F_0 = incident absorbed power densityW/m^2; ρ = density of the solid material kg/m^3; L = combined latent heat of

fusion and evaporation kJ/kg; C_p = specific heat of the solid material J/kg°C

T_v = boiling point at the pressure in the base of the hole °C; T_0 = starting temperature of the solid °C.

Table 1.1 presents the speed of penetration for a 2 kW laser beam. This value is of the order of 1 m/s and hence the velocity of the generated gas from this solid is of the order of 1000 m/s. The amount of material removed per pulse is directly proportional to the pulse length and energy supplied, with some 60% being removed as droplets due to the scouring action of the exiting gases.

Trepanning (cutting a tiny circle) or helical drilling (cutting in a spiral) is used to ensure parallel-sided holes. This also has the effect of reducing the

coincidence of the vapour and the beam (Hammersley G., Hackel L.A., Harris F. 2000).

Table 1.1 The calculated time for a 2 kW beam focused to 0.2 mm spot diameter. (Power density 6.3 $\times 10^{10}$ W/m^2) to raise the surface temperature to the boiling point. The table also shows the rate of subsequent penetration during laser drilling.

Material	Material properties				Process properties	
	Heat capacity, ρC_p (T_a-T_0) J/m3	Latent heat, (L_f+L_v) kJ/kg	Thermal conductivity, k (W/mK)	Thermal diffusivity, α (m^2/s)	Velocity of penetration, v (m/s)	Time to boil, t_0 (ms)
W	$1.6\text{x}10^{10}$	4205	164	6.07	0.64	3
Al	$5.9\text{x}10^{9}$	9889	226	9.3	1.9	0.6
Fe	$1.0\text{x}10^{10}$	6637	50	1.38	1.0	0.3
Ti	$7.6\text{x}10^{9}$	9437	19	0.81	1.2	0.09

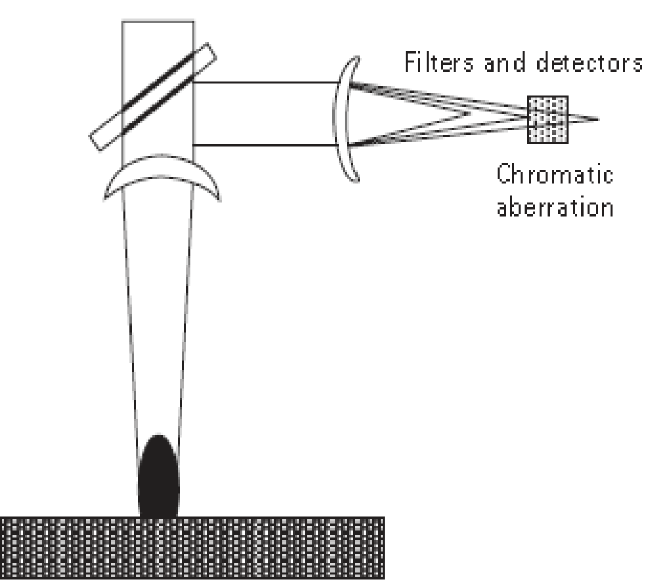

Figure 1.2. An arrangement for measuring the back reflection signal from the process. This signal can be used to detect the moment of full penetration during laser drilling and, if measurements are made of the red and blue frequencies from the laser generated plasma, it can be used as a signal on the focal position .

By observing the back reflected signals in an arrangement such as that shown in Fig. 1.2, it is possible to monitor the progress of drilling and hence stop the moment at which complete penetration has been achieved. This back reflected

signal is available at the output window from the laser and hence will be discerned on the back mirror of the laser. In fact the detector could be part of the laser machine, as developed by GSI Lumonics. This aspect of automating laser drilling is one of the attractive properties of laser processing.

Currently the laser is being used to drill holes in turbine blades, ink jet nozzles, micro vias in electronic circuit boards, irrigation pipes, baby’s teats, and nano holes in integrated circuits.

1.4.3 Laser welding

In laser welding the laser beam once again evaporates a hole into the material and then the ‘hole’ is traversed along the weld seam with the assist gas blowing gently to shield the weld pool from oxidation but gently enough to avoid disruption. The melt pool is subject to very large Marangoni forces due to the temperature gradients causing variations in the surface tension. It is also being pushed aside by the vapor hole where the laser is incident. The vapor hole or ‘keyhole’ causes the radiant power to be absorbed over the depth of penetration (by multiple reflections) – a form of line source, which is how laser welding is often mathematically modeled. The fusion profile is thus quite different from arc welding in that it has nearly parallel sides with a ‘nail head’ resulting from the hot vapors reradiating at the exit from the keyhole. However, the keyhole is only a hole in a liquid pool and is hence unstable. It opens and closes under the action of the vibrating melt pool and the Helmholtz instability in the throat of the hole – a form of venturi that closes as the velocity of the vapor from the hole increases. This together with the strong upsurge behind the keyhole can spoil the bead shape if frozen too quickly. The stability of the keyhole can be enhanced by using two beams to stop the keyhole closing. Twin beams have been used successfully when lap welding Zn-coated steels (Steen,and Mazumder 2010).

The depth of penetration and welding speed are both functions of the power density. The new generation of high brightness lasers seemed like the perfect answer to give a dramatic improvement in laser welding possibilities.

Unfortunately, although the above is correct, the weld width is very narrow and hence seam tracking is difficult. This can be overcome by broadening the weld pool through dithering the beam – as with a spinning beam [Harris and Brandt (2002)] – or by adding an electric arc to the laser for very little extra capital cost. The arc naturally locates with the laser generated plasma for low arc currents (up to 100 A); at higher arc currents the two heat sources act independently due to the high cathode jet velocities.

One aspect of laser radiation, which is different from most other forms of energy, is that it can pass through transparent materials. Taking advantage of the transparency of many materials to certain frequencies the welding of plastics has been developed using a transparent plastic lap welded to an absorbing plastic or a plastic that has been coated with an absorbing film (Hilton P.A., Jones I.A.,and Kennish Y 2002). Another example of the use of transparency is in underwater welding. Feeding the power to a diver via an optical fiber is considerably simpler than underwater arc welding; depths of up to 500 m have been achieved. One of the major applications has been in welding tailored blanks for the car industry. The laser is used because of the good cosmetic appearance of the weld bead, tolerance to changes in thickness and material; the speed of processing and lack of distortion in the resulting weld. The lack of distortion has also made the laser an attractive tool in ship building.

Recently a laser firing into a small glove box has found a large market amongst jewellers, who can weld rings and small articles which they hold by hand while watching through a microscope. Never before have jewelers been able to replace claws on rings without taking the stone out first.

1.4.4 Laser cladding

The laser is an ideal surface treatment tool. It can deliver almost any required thermal experience to a surface from mild bio-stimulation for relieving rheumatism to the generation of solid state plasmas as in laser peening) see Section 1.4.8). One of the current growth areas is in laser cladding. Cladding

can be done in a variety of ways, which differ in the manner of delivering the material to be melted as a clad. The material can be delivered as a powder, wire, sheet, foil or gas (the gas route can be a form of laser chemical vapor deposition). In all the melting processes the melt pool is vigorously stirred by the Marangoni forces caused by the steep thermal gradients (boiling point to melting point in the width of the melt zone).

One of the more successful cladding systems is based on blowing the powder into the laser-generated melt pool. This technique can give fusion-bonded clad layers having low dilution with the substrate. It was found that by cladding repeatedly in one location a wall could be created and that this wall had its grain growth up the height of the wall; a far stronger metallurgical configuration than that of a casting where the grains run across the wall thickness.

If instead of casting a straight wall, the clad track followed one layer after another in a 3D object calculated within a computer; then a 3D object can be cast directly without the need for a mould. Furthermore, the composition of the wall can be made to vary as the casting proceeds. Laser direct casting is one of the most flexible casting techniques possible (Mazumder J., Dutta D., Kikuchi N. et. Al. 2000).

1.4.5 Laser scabbling

This is another innovative laser process. In scabbling roads, heavy rolls with claws are scraped across the road surface and the top layer removed prior to resurfacing. In laser scabbling the objective is the removal of the top layer of concrete or plaster in the decommissioning of nuclear power stations, etc.; the top layer being the layer that contains most of the hot radiation or contamination. They found that a sufficiently powerful (several kW) laser spot of a few centimeters diameter scanned over the surface of a brittle material will cause explosive ejection of the top centimeter layer. The cause of this reaction is not precisely known but is a function of the thermal

expansion forces and possibly the steam pressure from the humidity within the structure (John C. Ion 2005).

1.4.6 Laser bending

This is another process that depends on thermal stress. As the top layer of a metal is heated, it will try to expand, but if the area heated is small then the surrounding material will restrain this expansion and eventually cause some plastic deformation, since at high temperatures the material is softer. On cooling, the stress builds up again because the material is now too short where it had been plastically distorted, but now the temperature is cooler and the material stronger, so it does not plastically revert, instead the material is gently bent towards the laser along the heated line by a few degrees for each pass of the laser. This process is known as the 'Thermal Gradient Method' (TGM) of laser bending. An alternative is 'Buckling' in which the expansion due to the laser heating occurs right through the sheet thickness and so a buckle or pimple forms. This buckle can be led along any line by the laser movement. Buckling is a faster bending process than the TGM and can cause bending both towards the laser and away from the laser depending on some prior tendency. A third method is that of 'upsetting' in which the laser heats through the sheet but the sheet is held rigidly and not allowed to buckle. In this case, plastic deformation occurs through the sheet, causing a shortening of the component on cooling. Some of the shapes that are possible have been illustrated by (Sarah Silve 2000). In one sample she was able to narrow the diameter of a tube (Fig. 1.3) while at the same time increasing the wall thickness.

Figure 1.3 An example of laser bending being used to narrow a pipe while at the same time thickening the walls in the narrow section (Sarah Silve 2000)**.**

1.4.7 Laser cleaning

Short sharp pulses of radiant energy can clean a surface; for example, remove the debris on electronic circuits, grime on statues or oxide films on welds in jewellery. How this is done is still a topic of discussion but it works and works well. In Greece the FORTH laboratories can clean paintings and use the laser spark that is part of the process to analyze what is being removed. There is a problem with cleaning pictures since some pigments can be bleached by radiation. The laser removal of the outer hardened varnish is sometimes useful.

The mechanism is thought to be via one or all of three mechanisms:

1. Evaporation – a 6 ns pulse of 0.2 J = 30 MW usually sufficient to evaporate most small particles.

2. Photochemical – The photon energy from a Nd:YAG laser at 1064 nm is 1.16 eV, while that from an excimer at 249 nm is 4.98 eV. This is more than the bonding energy between atoms in many organic materials. For example, the bond energy for a C–H bond = 3.5 eV. Therefore direct bond breaking is likely. Most dirt is held by far weaker Vander Waal bonds and so these bonds are likely to be broken by the radiation, allowing the dirt to be blown away.

3. Mechanical

(a) Photon pressure; the avalanche of photons in a kW laser beam can exert a minute force of a μNewton or so. When this force acts on a small focal spot the pressure can be significant.

(b) Expansion pressure: The sudden expansion of the substrate or particle can be similar to a minor earthquake from the particle's perspective and may shake it free of the surface from where it can be blown away. The oblique beam can remove surface debris from electronic boards very swiftly and more effectively than by direct normal radiation (Lee J.M. 2002)

(c) Recoil pressure or ablation pressure: the acceleration caused by thermal expansion under a short pulse is sufficient to cause material to fly away from a surface.

Laser cleaning has many advantages:

1- It is quiet process.

2- It does not require solvents or abrasive particles.

3- Its fume is easily collected by vacuum cleaning technology.

4- It sterilises as it cleans.

5- Metal cleaned by laser does not always need flux for subsequent soldering.

6- Spectral monitoring is possible.

1.4.8 Laser shot peening

When a powerful laser pulse strikes a wet surface there will be a plasma generated at the surface and the pressure confined due to the water damping layer. The result is a compression wave similar to that caused by a high velocity shot pellet. Provided the pulse is sufficiently short (ps) and powerful

drilling will not occur; there will only be a massive plasma ball that will generate pressure but block the beam from other surface damage: in fact create a knock on the surface like a pellet (Hammersley G., Hackel L.A., Harris F. 2000).

The advantages of this process are:

1- It creates a compressive stress in a surface that gives better fatigue life the main purpose of peening.

2- An improvement in resistance to fretting, galling and H embrittlement.

3- Stress corrosion cracking and inter-granular corrosion are reduced.

4- Some level of grain refinement can be achieved.

Problems with conventional shot peening are: a slight surface roughening; risk of embedded particles; difficulty in treating corners due to the geometry; the shot must be collected after processing, cleaned, graded and recycled; there is heavy wear on the machinery used; shot may become contaminated (e.g. radioactive). By contrast, laser peening gives the same level of compressive stress as conventional peening. The applications are in: aerospace–especially engines, automobiles, medical instruments, petrochemical plants, power plants.

1.4.9 Laser heat treatment

Heat treatment using lasers is a process that consists of heating metals and certain other materials for some time to harden them against wear with little or no distortion of other parts of the workpiece. Tools and automobile parts, for instance, are almost always heat-treated. For example, the ring grooves of the automobile piston can be hardened with a laser, without any distortion to the rest of the piece.

To obtain proper hardening, the temperature of the workpiece surface is raised above a critical temperature, followed by a particular cooling down stage. During heat treatment, it is important to control of the time evolution and intensity of the laser beam. The optimal irradiance distribution is determined by the thermodynamics of the laser-material interaction and by the shape of

the object, but typically, intensities between $5x10^2$-$5x10^3$ W/cm^2 are used for thermal annealing.

In general, CO_2 lasers are used for laser heating of metals. As they emit in the infrared (λ=10.6μm) and can operate either in the CW or pulsed mode, they are the laser of choice for heat treatment. However, since the reflectance of metals is very high in the infrared (λ=10.6μm), to reduce the reflectance and achieve adequate absorption, the surface of the workpiece is covered with an absorptive coating, such as black spray paint or graphite (John F.Ready 1997).

1.4.10 Laser Hardening

The principle of laser hardening is the irradiation of material surface for a short time.

Heat is conducted into a metal causing quick heating of a thin layer. During the heating period, a high temperature gradient is built up in the surface zone followed by a rapid self-quenching by the cool sub-surface material. The complete hardening d cycle takes about 1 to 2 s. The conventional surface hardening processes, such as flame hardening or induction hardening, often cause an amount of distortion so that the work becomes waste or there are high additional costs.

Medium and high carbon plain steels more than 0.3 per cent carbon are generally well suited to laser hardening. Their maximum hardness is a function of their carbon content. Mount of alloying elements, such as chromium manganese or molybdenum increases the hardenability. The advantage of laser hardening of steels is the possible substitution for expensive alloy steels. With the development of new techniques, lasers are now also being used to harden several other industrial products.

Normally for hardening a track width few millimeters, an output of more than 1 kW from the laser is considered desirable. Recent many laboratories engaged in laser application and research work all over the world, multi watt lasers have been installed. For heat treatment and hardening, usually a

continuous wave beam from a carbon dioxide laser is used (John F.Ready 1997).

1.4.11Velocity Measurement

It is well known that when a light beam gets scattered by a moving object, the frequency of the scattered wave is different from that of the incident wave; the shift in the frequency depends on the velocity of the object. Indeed, if υ represents the light frequency and v represents the velocity of the moving object which is moving at an angle θ with respect to the incident light beam (see Fig. 1.4), then the change in frequency $\Delta\nu$ between the incident and the reflected beams is given as $\Delta\nu$

$$\frac{\Delta\nu}{\nu} = \frac{2V}{c}\cos\theta \ldots\ldots\ldots\ldots\ldots\ldots\ldots\ldots\ldots\ldots (1-2)$$

Where c represents the velocity of light in free space. Thus the change in frequency $\Delta\nu$ is directly proportional to the velocity v of the moving object; this is known as the Doppler shift. Thus, by measuring the change in frequency suffered by a beam when scattered by a moving object, one can determine the velocity of the object. This method has been successfully used for velocity determination of many types of materials from about 10 mm/min to about 150 m/min (K. Thyagarjan and Ajoy Ghatak 2010). Further, using the above principle, portable velocity-measuring meters have been fabricated which measure speeds in the range of 10–80 miles/h; these have been used by traffic police. Laser Doppler velocimeters have also been used for measuring fluid flow rates.

The basic arrangement for velocity measurements is the following: the beam from a CW laser usually a helium–neon laser is split by a beam splitter; one of the components is reflected back from a fixed mirror and the other component undergoes scattering from the moving object. The two beams are then combined and made to interfere as shown in Fig. 1.4, and because of the

difference in frequency between the two beams, beating occurs. The beat frequency is a direct measure of the velocity of motion of the object.

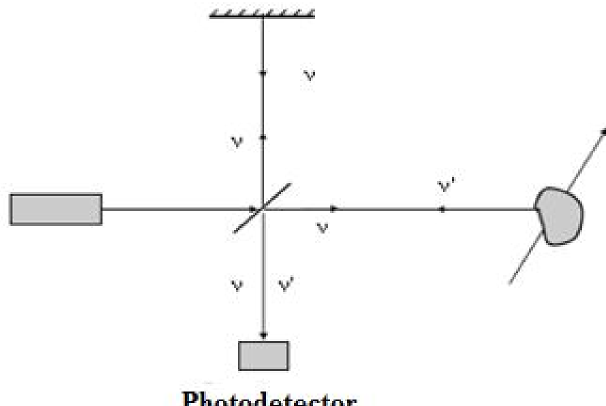

Figure 1.4 Schematic of an arrangement for measuring the velocity of a moving object using Doppler shift.

1.4.11.1 Lasers in Information Storage

Lasers find widespread applications in the storage, transmission, and processing of information. With progress in lasers and materials, the capacity of information storage has been steadily rising and today CDs are used to routinely store gigabytes of information.

Compact discs store information in digital form. Any form of information is first converted into digital form with just a sequence of 1s and 0s. In a CD these 1s and 0s are recorded in the form of pits or depressions along a spiral track on a plastic material with a metal coating (see Fig. 1.5). The total length of the track would be about 6 km. The usual coding is such that any transition from pit to land (flat area) or land to pit is read as 1s, while the duration in the pit or in the land is read as 0s (see Fig. 1.6). In CDs the radial distance between adjacent tracks, which is the track pitch, is 1.6 µm, while the length of data marks is about 0.6 µm. In order to write on the CD, the data stream is used to generate pulses of light corresponding to the data stream. The laser which emits an intense beam of light is focused on the surface of the CD

using an objective. As the CD rotates under the laser spot, a small region heats up whenever the laser beam hits and changes the reflectivity of the surface. Digital video discs (DVDs) use the same principle except that the track pitch is about 0.74 μm instead of 1.6 μm and the data marks are narrower and the focused laser spot is also smaller (see Fig. 1.7). The data are written on the CD along a spiral track on the surface. To read the information stored in the CD, a laser beam is focused through a beam splitter on the disc and the spot size of the focused laser is about the track width (see Fig. 1.8). As the CD moves under the focused laser spot, it leads to a modulation of the reflected intensity, which is then directed by the beam splitter to a photo detector which converts the intensity variations to electric current variations for further processing.

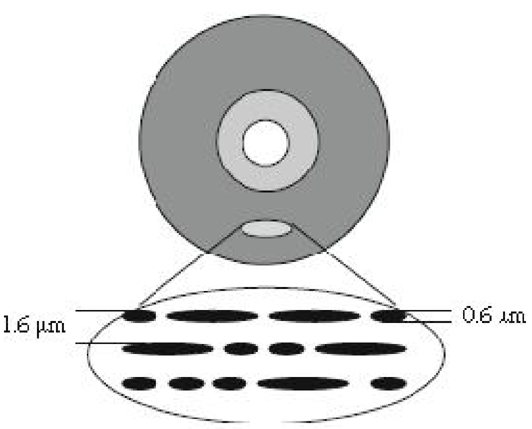

Fig. 1.5 In a compact disc (CD), information is stored in the form of pits along a spiral track

For writing and reading of the data, we use lasers and the minimum spot to which the laser can be focused will determine the size of the data points so that the readout can be precise. The fundamental limitation to the size of the focused spot of a laser beam arises due to diffraction. Smaller spot sizes can be achieved using smaller wavelengths and smaller focal length lenses. Since the CD is covered by a protective layer, the focusing need to be carried out through the protective layer and this determines the smallest focal length that can be used. A CD uses a 1.2-mm clear substrate and data are recorded on the

recordable layer through the clear substrate. The substrate also acts as a protective layer for the data. The reading wavelength is typically 780 nm.

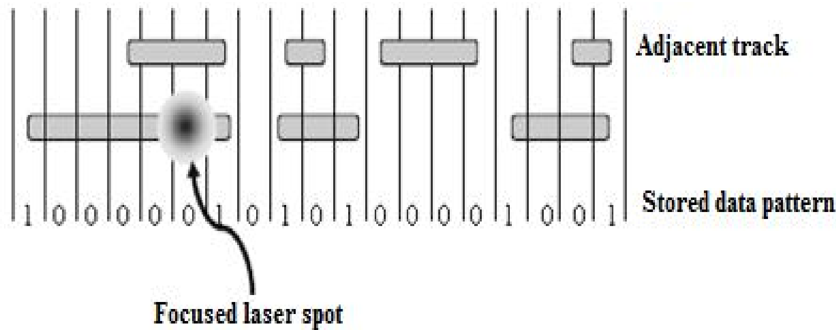

Fig. 1.6 In a CD, transition from land to pit or pit to land is read as "1s," while the duration within the pit or the land is read as "0s"

In contrast, in a DVD, two clear substrates each of 0.6 mm thick are bonded capacities since they operate with smaller wavelength and hence can be together and data are recorded on the bond side of each substrate. The reading wavelength in DVDs is typically 650 nm (see Fig. 1.9). Thus DVDs can store much more data than do CDs. Recent developments of blue lasers emitting a wavelength of 405 nm have triggered development of DVDs with much higher focused to smaller spot sizes. Table 1.2 lists a comparison of CDs, DVDs, and Blue Ray DVDs with regard to some important characteristics.

Table 1.2 Comparison of various parameters of CD, DVD, and Blue Ray DVD

Parameter	CD	DVD	Blue Ray DVD
Laser wavelength (µm)	0.78	0.65	0.405
Track to track spacing (µm)	1.6	0.74	0.32
Spot size of focused spot (µm)	1.6	1.1	0.48
User capacity (Gb)	0.68	9	50

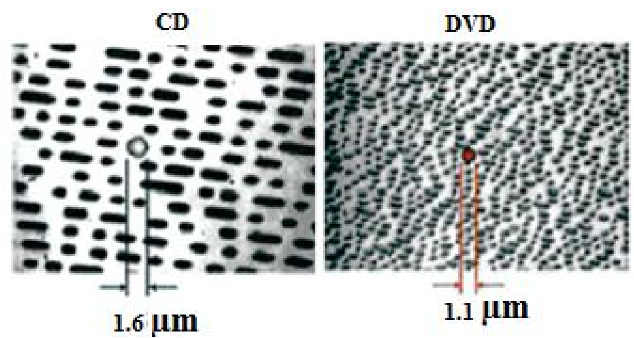

Fig. 1.7 Comparison between the pit sizes in a CD and a DVD

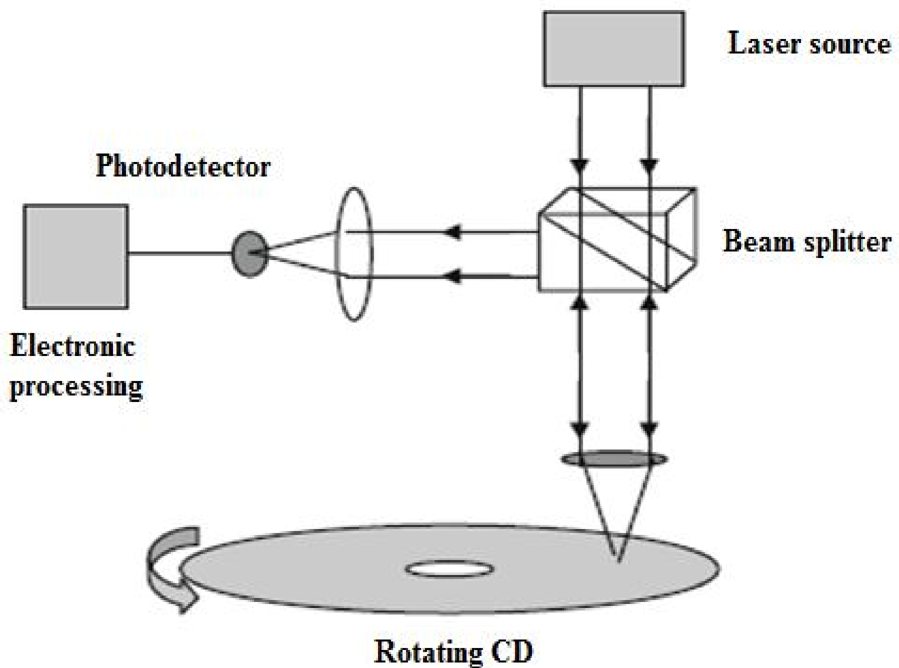

Fig. 1.8 A laser beam is focused on the CD and the reflected intensity is read and converted into the signal

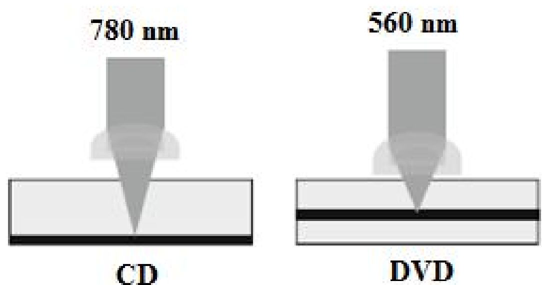

Fig. 1.9 Reading of a CD at a wavelength of 780 nm and a DVD at a wavelength of 650 nm.

1.4.11.2 Bar Code Scanner

The technology associated with identification of all types of products using bar codes is one of the very important developments of the past century. A bar code consists of a series of strips of dark and white bands (see Fig. 1.10). Each strip has a width of about 0.3 mm and the total width of the bar code is about 3 cm. Information such as the country of origin, manufacturer of the product, the direction of scan, price, reading error checking, weight of the product, and expiry date can be stored in the pattern of dark and white strips. By a simple scanning, complete information regarding the product can be obtained.

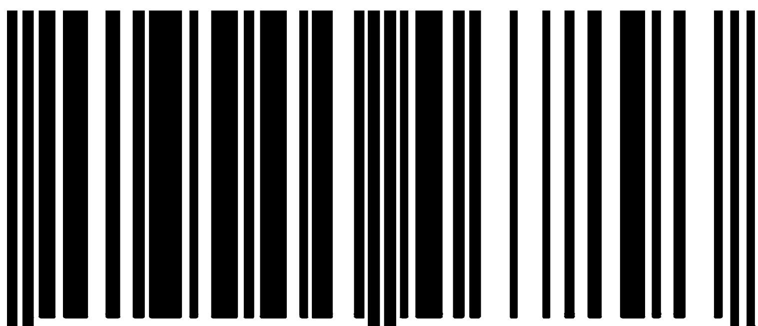

Fig. 1.10 A bar code consisting of series of strips of dark and white bands

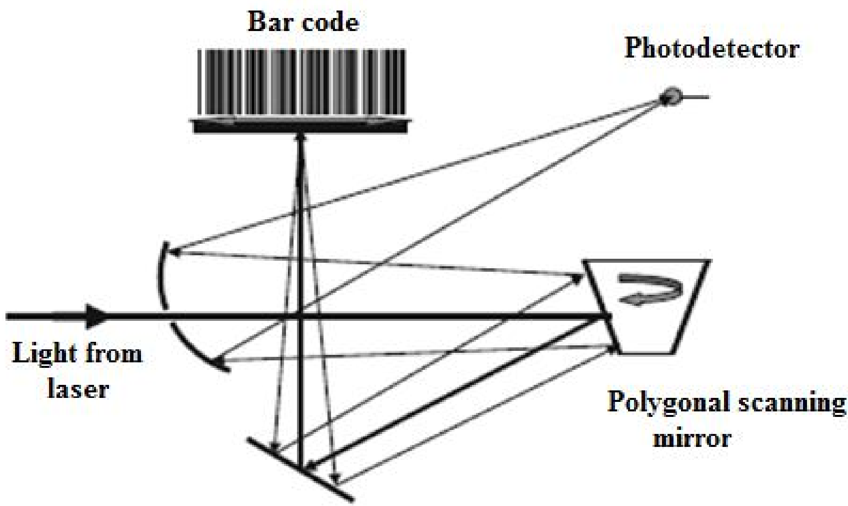

Fig. 1.11 A laser beam is scanned across the bar code and the scattered light is focused on a detector which converts the code into information

The basic role of the laser in this application is the optical reading of the bar code. A laser power of (~ 0.5 mW) with scanning speed of 200 m/s is deflected by a rotating polygon mirror to scan along a line (see Fig. 1.11). When the laser beam hits the bars, the amount of scattered light depends on whether the strip is black or white. As the laser beam scans across the black and white strips at a certain speed, the variation of scattering with time contains the information of the bar code. The scattered light is focused on a photo detector which converts the optical signal to an electrical signal for further processing. In order to be able to scan the product in any arbitrary direction for ease of scanning, the laser beam is made to scan in multiple directions by using multiple mirrors with the rotating polygon (K. Thyagarjan and Ajoy Ghatak 2010).

1.4.12 Precision Length Measurement

The large coherence length and high output intensity coupled with a low divergence enables the laser to find applications in precision length measurements using interferometric techniques. The method essentially consists of dividing the beam from the laser by a beam splitter into two portions and then making them interfere after traversing two different paths (see Fig. 12). One of the beams emerging from the beam splitter is reflected by a fixed reflector and the other usually by a retroreflector mounted on the surface whose position is to be monitored.

The two reflected beams interfere to produce either constructive or destructive interference. Thus, as the reflecting surface is moved, one would obtain alternatively constructive and destructive interferences, which can be detected with the help of a photodetector. Since the change from a constructive to a destructive interference corresponds to a change of a distance of half a wavelength, one can measure the distance traversed by the surface on which the reflector is mounted by counting t he number of fringes which have crossed the photodetector. Accuracies up to 0.1 μ m can be obtained by

using such a technique. This technique is being used for accurate positioning of aircraft components on a machine tool.

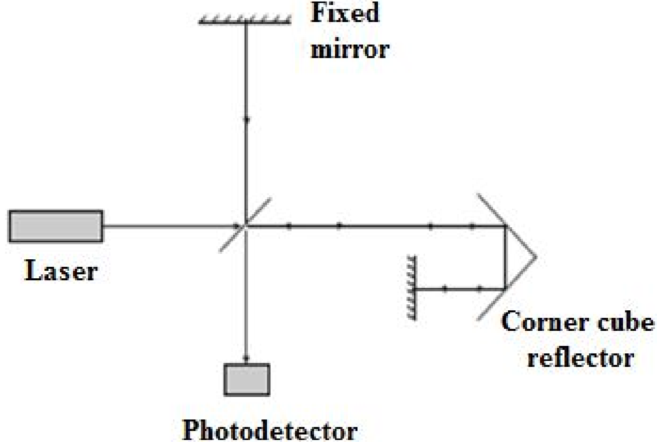

Figure 1.12 Laser interferometer arrangement for precision length measurements.

The conventional cadmium light source can be used only over path differences of about 20 cm. With the laser one can make very accurate measurements over very long distances because of the large coherence length. The most common type of laser used in such applications is the helium laser and since the distance measurement is being made in terms of wavelength, in these measurements, a high wavelength stability of the laser output must be maintained (K. Thyagarjan and Ajoy Ghatak 2010).

1.4.13 Laser Alloying

Surface alloying involves spreading of a powder containing alloying elements over the surface to be hardened. Then, the laser beam traverses the surface. The powder and a thin surface layer melt and intermix. After passage of the beam, the surface resolidifies rapidly. A thin layer containing the alloying elements remains, with hardness greater than that of the original material. An alternative method of supplying the alloying elements uses a gas jet to blow the powder onto the melted surface.

The laser typically is a multikilowatt CO_2 laser in order to achieve coverage of large areas. The treating rate is somewhat slower than for transformation hardening, because some surface melting is required.

Surface alloying can produce surfaces with desirable properties on relatively low cost substrate materials. For example, one could produce a stainless steel surface on low carbon steel by alloying nickel and chromium.

Alloying requires a high value of heat input, controlled to produce the desired depth of surface melting. A laser is the only practical heat source for surface alloying.

In one study, the elements carbon, boron, chromium, and silicon were mixed in powder form on the surface of a valve seat. The powder was melted and alloyed into the surface by an 18-kW CO_2 laser beam. The treating and surface hardening took less than 1.5 sec for a valve seat (John F.Ready 1997).

1.4.14. Laser glazing

Laser glazing involves some surface melting. As the beam from a multi kilowatt CO_2 laser is scanned over a surface, a thin melt layer is produced under proper conditions of irradiance and traverse speed. The interior of the workpiece remains cold. After the beam moves on, resolidification occurs very rapidly. The surface layer is quickly quenched. As a result of this process, one may produce surface microstructures with unusual and possibly useful characteristics. The grain size near the surface is very small, because of the high quench rate. The surface structure can appear glassy; hence, the name laser glazing. This technique is applicable both to metals and ceramics. It appears to be controllable and reproducible.

Laser glazing can produce surfaces that are amorphous or that have a glassy, non crystalline structure. Such surfaces can have increased resistance to corrosion.

One example of laser glazing is surface melting of cast iron with rapid

resolidification. This produces a thin surface layer of very hard material called white cast iron, which can provide excellent wear resistance. Another example that has been demonstrated is the glazing of aluminum bronze, which leads to surface structures with enhanced corrosion resistance (John F.Ready 1997).

CHAPTER TWO

Laser Micromachining and Annealing

2.1Introduction

Historically, laser annealing has been viewed as a means of eliminating ion implantation damage associated with doping in semiconductors. Both CW radiation and pulsed laser radiation have been shown to be effective in annealing out this damage with little or no degradation of the substrate. This early work was primarily carried out with CW Ar or Kr, Nd:YAG and ruby lasers (W.W. Duley 2005) In this chapter, P-N junction fabrication, diode resistances, applications of laser in micromachining, basics of laser annealing and literature review of annealing of electronics devices are explained.

2.2 Fabrication of PN-Junction Diode by IC Fabrication process

The advent of integrated circuits made it possible to place a number of transistors and thus an entire circuit on a single chip. In the beginning these circuits had only few transistors but as the technology improved they became larger. Integrated circuits are manufactured on a silicon wafer. By 1970 it was possible to implement all circuitry needed to realize a microprocessor on a single chip. In the 1960s Gordon Moore predicted that the number of transistors that could be manufactured on a chip would grow exponentially (Shailesh siddha and Yashika Chander Pareek 2013).

2.2.1 Fabrication Facilities

To successful manufacture a very large scale integration (VLSI) circuit, it is necessary to control cleanliness, temperature, humidity and orderliness.

A. Pure water system: IC fabrication use large amount of water. Water contains impurities of sodium, copper and iron. These impurities can

deposit on wafer during processing. There is a need of ultra pure deionized water. Water with specific resistivity 18MΩ-cm is considered to have a low ionic content. The resistivity of water is monitored by electrical means and particulate in water are monitored by automatic light block type of liquid borne particle centre.

B. Clean room: All process steps are implemented in clean room. The air is maintained at a well controlled temperature and humidity level and is continuously filtered and re-circulated. Air in the clean room is monitored and classified with respect to particulate. A "class 100" environment has a maximum of 100 particles per cubic foot with particle size larger than 0.5μm and a maximum of 10 particle per cubic foot with particle size larger than 5.0μm particulate can emanate from process equipment as well as from human; personal must wear proper clothing to protect the wafer.

2.2.2 Fabrication Process

Diode is a basic element in electronic and digital circuit. In this paper formation a PN junction diode is explained by VLSI fabrication steps which are stated below.

2.2.2.1 Silicon wafer cleaning (RCA process)

In the IC processing wafers it is necessary to maintain the purity and perfection of material. Silicon wafer is cleaned by standard RCA process. It useful to remove oil/grease, organic/ionic contamination, heavy metal ion and native oxide from the surface of wafer. Oil/grease/dust is removed by boiling wafer in trichloroethylene (TCE), acetone and methanol. Organic/ionic contamination is removed by boiling wafer in $H_2O:NH_4OH:H_2O_2$ (5:1:1) solution. Heavy metal ion is removed by boiling wafer in H_2O: HCl: H_2O_2 (6:1:1) solution. Native oxide is removed by boiling wafer in HF: H_2O (1:50) solution. Silicon wafer should rinse with deionized (DI) water after each acid step.

2.2.2.2 Oxidation

Process by which a layer of silicon dioxide (SiO2) is grown on a silicon substrate is known as oxidation. This process is carried out in a furnace in high temperature. In this process dry wet dry oxidation is performed. When silicon wafers are heated in a pure oxidizing gas ambient such as dry oxygen it known is as Dry Oxidation. Oxide layers are very uniform but Dry oxide grows very slowly i.e oxidation rate is very low When silicon wafers are heated in an ambience of wet oxidizing gas such as oxygen bubbled through hot D.I Water (carrying steam vapors) it is known as wet oxidation. Growth rate is high but Quality of grown oxide is not very good. It is porous, i.e less dense compared to dry oxide.

Advantages of Silicon Dioxide in IC Technology: There are several advantages of silicon dioxide in IC-technology such as

1- Easily and selectively etched using photolithography techniques.

2- Excellent masking behavior with most of the common impurity species, such as boron, phosphorus, arsenic and antimony.

3- Excellent electrical insulator with resistivity values of the order of 1.0 X 10^{16} Ω-cm and a band gap of 9.0 eV.

4- Very high breakdown field, of the order of 1.0 X 10^{7} V/cm.

5- Excellent junction passivation.

6- Stable bulk electrical properties over a long period of time.

7- Highly stable and reproducible interface states of Si-SiO2 interface with silicon.

2.2.2.3 Photolithography

In I.C Technology, photolithography is used to transfer patterns made on a mask to a semiconductor wafer. Therefore, to fabricate a device or an I.C, the oxide layer needed to be removed from the Selective regions on silicon wafer, where diffusion is desired. First silicon wafer is coated with photo resist and exposed in ultra violet light. By the application of photo resist oxide layer is

etched . Photo resist is an organic polymer, sensitive to UV light. It is temporarily coated on wafer surface to transfer design image on it through exposure in UV light.PR is applied to the oxidized wafer using a spinner. Spinner has vacuum holding arrangement and very high acceleration motor having adjustable speed (2000 to 6000 rpm).

2.2.2.4 Oxide etching

To remove SiO_2 from regions exposed through photolithography is called oxide etching. After post bake, the wafer is dipped in Buffer HF solution for a particular time (determined by oxide thickness and etch rate) followed by thorough rinsing in D.I Water. It is called wet etching. To remove photo resist water cleaned wafer is boiled in acetone 2 min. to completely remove the photo resist from the wafer surface. If Wafer is subjected to Chemical Vapor Etching i.e subjected to a reacting gas mixture in a CVD reactor. It is called dry etching.

2.2.2.5 Diffusion

As the given wafer is N type so we need to diffuse P type impurity into the wafer to create P-N junction and we take Boron (P type) impurity for diffusion. Boron activation, pre deposition of boron and oxidation is going on. During boron activation a layer of B_2O_3 is formed on BN wafer. After that silicon wafer is placed with BN wafer and boron will diffuse into silicon wafer. During this process boro silicate glass is deposited so we need to etch the glass.

Glass etchant → 5ml BHF+85ml DI water+10ml HCl

BHF solution → 40gm NH_4F in 40ml of DI water+10ml HF

Material used for:

Antimony diffusion → Sb_3Cl_5 (antimony penta chloride)

Arsenic diffusion → As_2O_3 (arsenic tri oxide)

Phosphorus diffusion → $POCl_3$ (phosphorus oxi chloride)

2.2.2.6 Metallization

Metallization is the final step in the wafer processing sequence. Metallization is the process by which the components of IC's are interconnected by aluminum conductor. This process produces a thin-film metal layer that will serve as the required conductor pattern for the interconnection of the various components on the chip. Another use of metallization is to produce metalized areas called bonding pads around the periphery of the chip to produce metalized areas for the bonding of wire leads from the package to the chip.
Aluminum purity should be 5N (99.999%)

2.2.2.7 Photolithography

Photolithography is required for device isolation many devices can be fabricated in a single wafer. It is done by the same process as stated earlier photolithography process.

2.2.2.8 Metal Etching

Aluminum etching is done on the selective portion. It is done by the same process as stated earlier.
Aluminum etchant orthophosphoric acid

2.2.2.9 Annealing

First step in IC fabrication is to introduce dopant atom. Implantation damages the target and displaces atoms from its site.
The electrical behavior after implantation is dominated by deep level electron and hole traps, which capture carriers and make the resistivity high. Annealing is the process which is used to repair the lattice damage by putting atoms on substitutional sites where they will be electrically active (Shailesh siddha and Yashika Chander Pareek 2013).

2.2.3 Processing Effects

After fabrication, wafer may be divided into regions with a very high portion of good chips and other regions where the yield of good chips is very low or zero. These effects include variations in the thickness of oxide, in the resistance of implanted layers, in the width of lithography, defined features, and in the registration of photo mask with respect to previous masking operations. Region where the poly silicon layer is thinner than average become over etched. Variation in the doping can lead to variation in the contact resistance in implanted layer. Variation in the thickness of deposit dielectric can lead variation in contact window sie. As advanced processes are developed which can eliminate or reduce these effects?

2.2.4 Advantage

ICs have three key advantages over digital circuits built from discrete components:-

1- Size: Integrated circuits are much smaller—both transistors and wires are shrunk to micrometer sizes, compared to the millimeter or centimeter scales of discrete components. Small size leads to advantages in speed and power consumption, since smaller components have smaller parasitic resistances, capacitances, and inductances.

2- Speed: Signals can be switched between logic 0 and logic 1 much quicker within a chip than they can between chips.

Communication within a chip can occur hundreds of times faster than communication between chips.

3- Lower power consumption**:** Replacing a handful of standard parts with a single chip reduces total power consumption. Reducing power consumption has a ripple effect on the rest of the system: a smaller, cheaper power supply can be used; since less power consumption means less heat, a fan may no longer be necessary; a simpler cabinet with less shielding for electromagnetic

shielding may be feasible, too (Shailesh siddha and Yashika Chander Pareek 2013).

2.3 Diode Resistance

When some external voltage is applied across a diode, some current flows. Therefore, the diode can be imagined to have some resistive behavior. This resistive behavior of diode is generally called diode resistance. On the basis of type of applied voltage, diode resistance can be divided into two parts.

1- Static resistance or DC resistance.

2- Dynamic resistance or AC resistance.

2.3.1Static Resistance

The resistive behavior of diode in presence of DC source is called static resistance or DC resistance. It can be defined as the ratio of applied DC voltage across diode and its respective current.

i.e $r_{DC} = V_{DC}/I_{DC}$

2.3.2Dynamic Resistance

The resistive behavior of diode in presence of ac source is called dynamic resistance or ac resistance. On the basis voltage range of applied signal, dynamic resistance can be of two types.

1- r_{ac} (avg). It is applicable for large ac signal applied across diode.

2- $r_{ac.}$ It is applicable for small ac source applied across diode.

r_{ac} (avg) It is a dynamic resistance of a diode in the presence of large applied signal. It can be defined as

$$r_{ac}(avg) = , \frac{\Delta V}{\Delta I} , \ldots\ldots\ldots\ldots\ldots\ldots\ldots\ldots\ldots\ldots\ldots\ldots \quad (2-1)$$

ΔV is change in voltage across diode in presence of ac source. ΔI is change in current through diode in presence of ac source.

Dynamic resistance can also be calculated by graphical analysis based on diode characteristic.

2.3.2.1 Graphical analysis

For very small signal, points Q1 and Q2 on characteristics will shifted toward point Q and line between Q1 and Q2 will be converted into a tangent at point Q figure 2.1.

To calculate r_{ac} first of all find operating point (suppose it is at 0.8V in characteristics), then draw a tangent on diode characteristic at operating point. Now calculate slope of tangent at operating point. Dynamic resistance r_{ac}=1/slope of tangent at operating point.

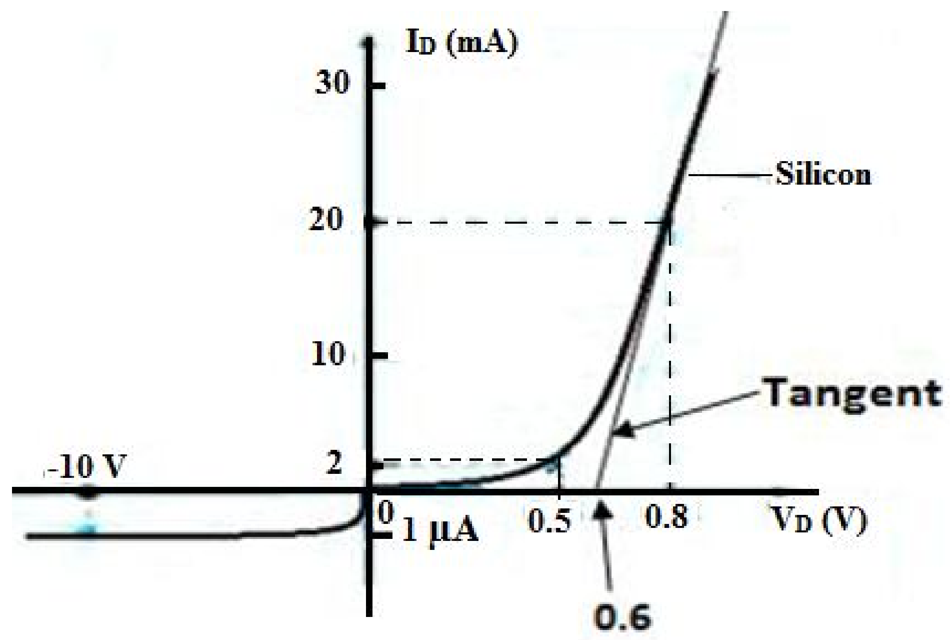

Figure 2.1. Current – Volt characteristic of silicon diode

In figure 2.1, slope of tangent will be 20mA/0.2V. So r_{ac} will be 0.2V/20mA=10Ω.

2.3.2.2 Mathematical analysis

Dynamic resistance of diode can also be calculated by mathematical equation. As we discussed that to calculate dynamic resistance slope of tangent at operating point is required. Slope of tangent at operating point $= \frac{dI}{dV}$.

We know

$$I = I_0\left(e^{\frac{V}{\eta V_T}} - 1\right) \ldots\ldots\ldots\ldots\ldots\ldots\ldots\ldots\ldots\ldots\ldots\ldots\ldots (2-2)$$

So $\frac{dI}{dV} = \frac{(I_0 e^{\frac{V}{\eta V_T}})}{\eta V_T}$

So $r_{ac} = \frac{dV}{dI} = \frac{\eta V_T}{(I_0\, e^{\frac{V}{\eta V_T}})} = \frac{\eta V_T}{(I+I_0)}$

Forward bias condition

$$r_{ac} = \frac{\eta V_T}{(I_0 e^{V/\eta V_T})} = \frac{\eta V_T}{(I+I_0)} \ldots\ldots\ldots\ldots\ldots\ldots\ldots\ldots\ldots\ldots\ldots\ldots\ldots (2-3)$$

For Reverse bias condition

$$r_{ac} = \frac{\eta V_T}{(I_0 e^{-V/\eta V_T})} = \frac{\eta V_T}{(I+I_0)} \ldots\ldots\ldots\ldots\ldots\ldots\ldots\ldots\ldots\ldots\ldots\ldots (2-4)$$

Where

I= diode current, I_0= reverse saturation current, η is the semiconductor constant =1 for Ge, 2 for Si, V_T=Voltage equivalent of temperature.

If the magnitude of reverse bias voltage is more than 0.5V, then the reverse current

$$I \cong I_0 \ldots\ldots\ldots\ldots\ldots\ldots\ldots\ldots\ldots\ldots\ldots\ldots\ldots\ldots\ldots\ldots\ldots\ldots\ldots\ldots (2-5)$$

So $r_{ac} = \frac{\eta V_T}{(I_0)} \ldots\ldots\ldots\ldots\ldots\ldots\ldots\ldots\ldots\ldots\ldots\ldots\ldots\ldots\ldots\ldots\ldots\ldots\ldots\ldots\ldots (2-6)$

For a forward bias diode, if $I >> I_0$ the $r_{ac} = \frac{\eta V_T}{(I)} \ldots\ldots\ldots\ldots\ldots\ldots\ldots (2-7)$

For example, if the forward current I = 52 mA, then the dynamic resistance

r_{ac} = for Ge $\eta = 1$, V_T = 26 mv at room temperature

Then rac = $\frac{26}{(52)} = 0.5\, mV$.

2.4 Laser micromachining

The need for micromachining of thin film resistors and thin film on silicon circuitry has led to several important industrial applications of lasers. The advantages of laser processing in this area include:

- Small heat affected zones

- Control over machining depth
- Rapid throughput
- Accomplishment of machining at any time during or after processing

2.4.1. Resistor trimming

Laser trimming of thin and thick film resistors has been able to be fundamental place in industry. Trimming is executed by vaporizing bit of the film or by thermally modifying bit of the film to alter its resistance. When vaporization is used, material may be removed either as a series of holes [Figure 2.2 (a)] or continuously in the form of lines [Figure 2.2(b)].

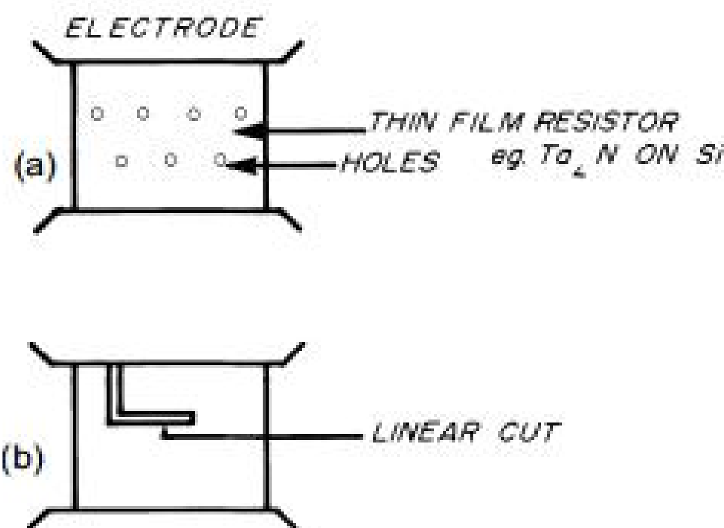

Figure 2.2. Resistor trimming by (a) removal of discrete areas and (b) by cutting lines.

Resistors are normally fabricated to lower resistance values than needed and trimmed by cutting holes in them with lasers to increase their resistance value. Various trimming patterns are used today to meet the desired trimming characteristics. Common practice is to use “L” shaped trims (“L-cut”) (see Fig. 2.3), where a cut perpendicular to the current flow in the resistor quickly increases the resistance to near the target value, then a change in direction of the trim to parallel to the current flow slows down the change in resistance to reach the target. Other common trimming patterns include “single-dives”: trimming straight into the material; “double-dives”: trimming straight into the

material in two locations; “serpentine” trims; as well as several other patterns and variations thereof, (Phillip Sandborn and Peter A. Sandborn 2008).

The Q-switched Nd-Y AG laser is the laser of choice in trimming thin film resistors. Typical operating parameters are

Pulse length 200 ns

Peak power 1-10 KW

Repetition rate 1 kHz

Repetitive Q-switching at high rates permits the generation of linear cuts by the overlapping of individual pulses. This is accomplished by scanning the beam at the rate of spot radius X repetition rate.

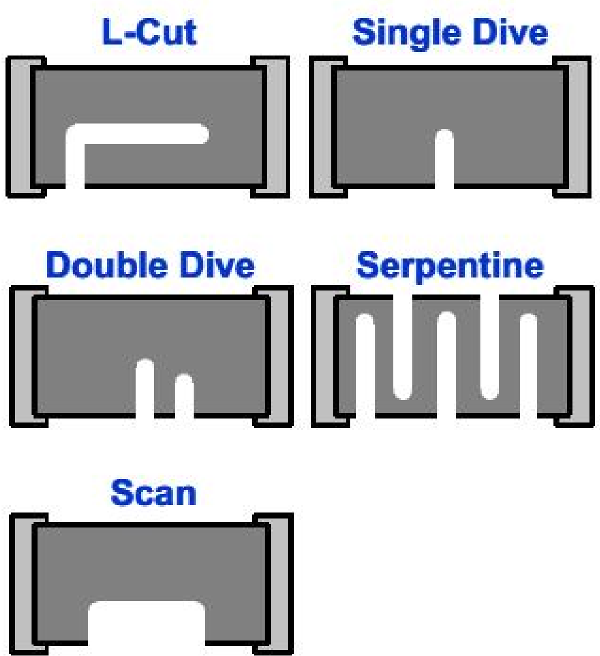

Figure 2.3 Various resistor trimming patterns.

For example, for a 20 -µm diameter spot size and a repetition rate of 1 kHz, the scan speed is

$$10 \text{ X } 10^{-6} \text{ X } 10^{3} = 10 \text{ X } 10^{-3} \text{ m S}^{-1} = 1 \text{ cm S}^{-1}.$$

The penetration of heat into the substrate can be roughly estimated from

$$\Delta x = (kt)^{\frac{1}{2}}$$

where Δx is the penetration, k the thermal diffusivity, and t the duration of laser pulse. When $k = 0.1$ cm^2 S^{-1} and $t = 200 \text{ X } 10^{-9}$ s, $\Delta x = 1.4 \text{ X } 10^{-4}$ cm.

Thus Q-switched lasers are ideal for the removal of limited amounts of material on thermally sensitive substrates.

Constraints on laser sources for trimming thick film resistors are slightly different from those with thin film devices. The greater volume of material to be removed requires higher energies per pulse and longer pulse lengths. This means that the pulsed CO_2 laser may be more suited than the Nd-Y AG laser for some applications in this area.

Comparison of CO_2 and Nd-Y AG sources must also take into account the effect of sample reflectivity. CO_2 laser radiation is strongly absorbed by many nonmetallic materials and is reflected from metals. At the Nd-Y AG wavelength (1.06 μm), many nonmetallic materials are relatively transparent. The reflectivity of metals at 1.06 μm is also smaller than at 10.6 μm so that Nd-Y AG radiation is more strongly absorbed in metals.

Some practical problems associated with laser machining of thin and thick film resistors. These problems relate to factors that can lead to drift and instability following trimming. Possible problem areas are shown in Figure 2.4.Insufficient laser power during trimming results in detritus in the cut. This may consist of islands of unevaporated material or random debris ejected from the sides of the cut. Thermal shock can lead to crack formation with subsequent instability during operation. Headley identifies the following common causes of drift and instability:

-Final current paths are too narrow leading to overheating.

-Trimming too close to a termination.

-Long kerfs in the direction of current flow.

-Machining that crowds current density into zones subjected to shock from processing.

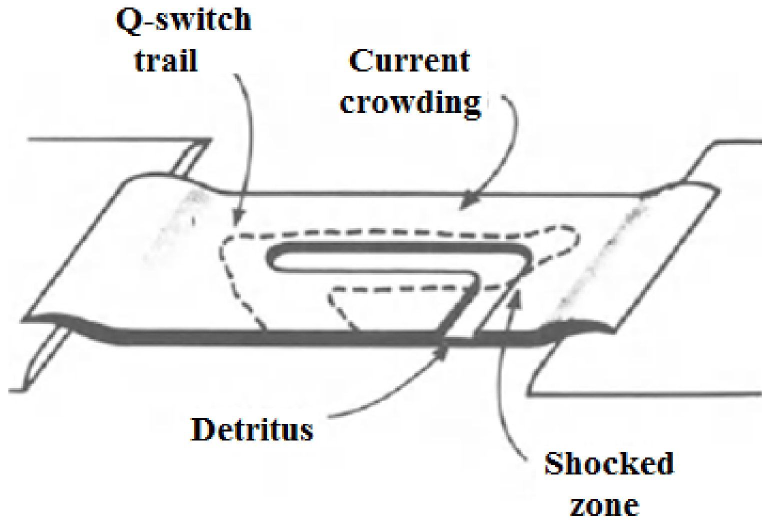

Figure 2.4. Possible problems in laser trimming of resistors. Detritus in the kerf, microcracks in the region surrounding the kerf, current crowding in the shocked zone (due to poor geometrical design), and Q-switched trail are the major potential sources of trouble in a laser trimming operation (W. W. Du'ley 1983)**.**

A significant development in laser trimming technology involves the trimming of elements in active circuits. A computer controlled laser can be combined with electrical measurements on the circuit to yield optimized circuit performance under dynamic operating conditions (W. W. Du'ley 1983)**.**

2.4.2 Laser direct –write

Laser direct-write (LDW) is a general term that encompasses modification, subtraction and addition processes that can create patterns of materials directly on substrates without the need for lithography or masks. The interaction of the laser with the substrate, or any other surface for that matter, results in material modification (melting, sintering, etc.) or material removal (laser micromachining). The later allows the generation of the trenches or pockets where the devices are to be embedded inside the substrate. Subtractive LDW can generate patterns by either moving the substrate or rastering the laser beam or a combination of both. In additive mode, the LDW technique behaves effectively as a "functional materials printer" as shown schematically in Figure 2.5. Simply stated, powders of the material to be

deposited, i.e. Ag powders (to make electrically conductive metal patterns), are combined with a liquid carrier to form an ink. This ink is spread on a glass plate to form what is referred to as the ribbon. The ribbon is held above the substrate surface separated by a distance of 100 to 200 µm so it can move independent of the substrate. A pulsed UV laser (DPSS Nd:YVO4, 355 nm, 30 n sec) irradiates the ink from behind the glass plate to propel a mass of material forward to the substrate below. This laser printing process takes place by rastering either the beam or the substrate to produce a pattern of material. Different materials can be deposited by simply changing the composition of the ribbon (Alberto Piqué , Bhanu Pratap, Scott A. Mathews et. al. 2007).

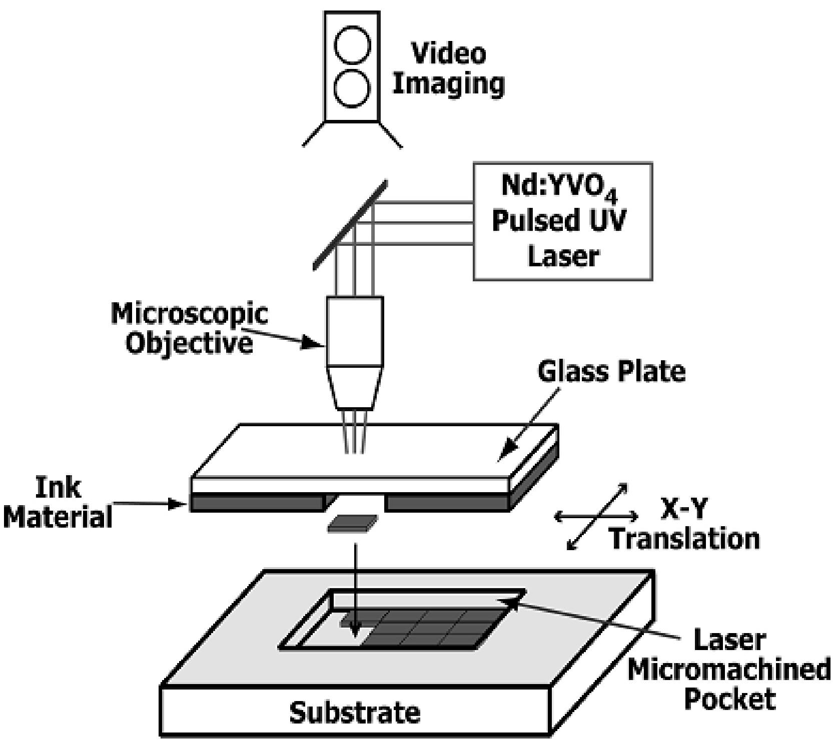

Figure 2.5. Schematic of laser direct-write addition process showing deposition within the substrate.

2.4.3 Laser marking

Product laser marking is one of the most common industrial applications of lasers. The laser marking systems using different lasers and optical delivery systems may be used to mark an almost endless list of materials including

metals, plastics, ceramics, glass, wood and leather as well as painted surfaces and photographic emulsions. Laser marking most commonly takes the form of an alphanumeric code imprinted on the surface of the product to indicate the date of manufacture, best-before, serial number etc. Laser marking is superior in quality and flexibility to traditional marking techniques; it leads itself to automation and integrated production techniques. The common advantages of all laser marking techniques are:

1- permanent, high quality marks;

2- High efficiency and low operation cost;

3- Good accessibility, even to irregular surface;

4- non-contact marking and no special working environmental needed;

5- Easy to automate and integrate (direct writing of patterns can established using computer-controlled movement of the beam or sample);

6- Precise beam positioning and a beam highly localised energy transfer to the workpiece;

7- High reproducibility and high speed.

8- Contamination - free.

2.4.3.1 Laser marking mechanism

The marking processes include one or a combination of the following processes (table 2.1):

- black carbonisation;
- bleaching or changing the colour of a colorant in the material;
- physical modification of the surface finish;
- scribing a shallow groove into the material by vaporisation;
- highly-controlled modification of the surface by melting.

Table 2.1 Laser marking technologies

Process	Schema		Mechanism
Vaporization			Material removal mainly by vaporization
Thin layers material removal			Thin layers material removal by controlled vaporisation, changing the colour of the under layers
Carbonisation or coloration			Colour changing by photo-thermal or photo-chemical reactions
Surface modify by material fusion			Destruction of materials by pyrolyze reaction that leads to irregular structures into the material

Briefly, it comes out that the laser marks are created by vaporizing, melting or annealing the material. Each has a specific effect for different marking applications. Vaporization produces a mark with depth in the material, like engraving. Melting creates a contrasting mark through a thermal-chemical reaction. This technique is often used with plastics. Annealing the surface of a material, such as steel or titanium, can produce a dark mark without noticeable surface penetration (Adelina Han and Dinu Gubencu 2008).

2.4.4 Hole drilling

The straight forward application of laser ablation in micromachining is hole drilling. In the simplest form it is accomplished by focusing a laser beam onto the workpiece and applying as many pulses as required to obtain via hole (through hole) or a pocket hole (blind hole). With this method a reasonable quality of the holes is obtained only, if a Gaussian laser beam is used, e.g., in the case of solid state lasers (YAG). In the case of flat top beam profiles

(excimer laser), perfect quality can be achieved by mask imaging. Depending on laser energy, size of the hole and material, one hole at a time is made with a pinhole mask, or parallel processing of a multi hole pattern is performed using a complex multi hole mask.

An important application of micro hole drilling is the fabrication of nozzle plates for ink jet printers. In a standard process, several rows of holes are drilled simultaneously using an excimer laser and a mask projection system. These holes in polyimide have diameters of about 10–50 µm. In such configurations, it has to be taken into account, that even in the case of homogeneous illumination, nonuniform hole depths are obtained due to geometrical effects of the plume shielding. Depending on the required geometries, materials and hole dimensions, holes in multilayer printed circuit boards are made by excimer laser drilling , or for instance in a combined process, where copper layers are drilled with a frequency tripled YAG-laser and the intermediate dielectric layers are removed by a CO_2-laser. Using CO_2-lasers, hole dimensions down to 10 µm are possible in polyimide and glass material.

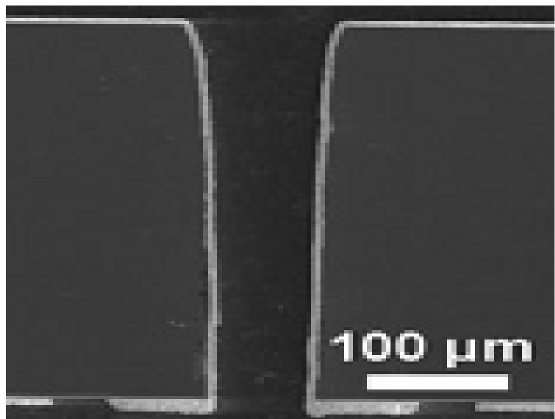

Fig. 2.6 355 nm-laser drilled hole in SiC after etching and metallization.

Also in semiconductor device fabrication and production of photovoltaic devices there are several applications of hole drilling. One example is the drilling of silicon carbide wafers. Using a frequency tripled diode pumped

solid state laser at 355 nm, through and blind holes of 60 µm diameter with aspect ratios of 5–6 have been obtained (Fig. 2.6). For the back contacting of solar cells, processes with parallel drilling of up to 5,000 holes using 1,047 nm-laser radiation have been developed.

Fuel injection nozzles in steel for gasoline or Diesel engines with typical diameters of around 100µm are made mainly by diode pumped YAG-lasers, either with the fundamental wavelength or using the second or third harmonic. Not only size reduction but also specifically shaped holes (tapers) are of interest. Other applications of laser hole drilling are in the biomedical field. One example is the fabrication of nozzles for the so called pulmonary drug delivery. These nozzles often have to be strongly conical with an exit diameter of about 1µm. Excimer lasers are used to fabricate such disposable nozzle plates (Peter Schaaf 2010).

2.5 Laser Annealing

One of the most dynamic areas of laser application over recent years has been that of laser annealing of ion-implantation damage in semiconductors. The implantation of ions of B, As, or P in a semiconductor such as Si leads to the formation of thin surface layers with *p*- or n-type characteristics. Since this implantation is accomplished by accelerating ions to keV energies before impact on the semiconductor surface, doping by this method is accompanied by damage to the host crystal. This damage takes the form of dislocations, stacking faults, dislocation loops, and a variety of point defects. At the doses customarily used for doping, this damage may be sufficient to drive the ion-implanted layer amorphous. Furthermore, many impurities do not end up in substitutional lattice sites and are not available for electrical conduction. This damage can be partially removed by thermal annealing, i.e., by heating the entire semiconductor in a controlled atmosphere in a furnace. However, this rather drastic treatment often leads to contamination and degradation of

electrical performance. In addition, bulk heating can lead to diffusion and recombination of dopants with precipitation in some instances.

Laser annealing of the ion-implanted layer has been shown to overcome many of these limitations. In particular, since laser annealing heats only the damaged layer, no degradation of the substrate is produced. Heating with pulsed or CW lasers yields essentially complete recrystallization of implanted layers with little residual damage and no diffusion of impurities. Dopant atoms are also observed to exclusively occupy substitutional lattice sites following laser annealing. Table 2.2 lists some semiconductors that have been subjected to laser annealing.

Although many of the drawbacks of thermal annealing are removed with laser annealing, others characteristic of the new process occur. For example, with pulsed laser annealing the semiconductor surface may become irregular and stresses may be introduced at the interface where melting terminated. With CW annealing some defects may remain.

Table 2.2, Laser Applications in Semiconductor Processing and Device Manufacture

Laser Applications
Annealing of ion-implantation damage
Recrystallization of amorphous layers
Laser-assisted doping
Ohmic contact formation
pn Junction formation
Silicide formation
Production of metal-semiconductor contacts in MOS structures
Machining of monolithic displays
Modification of resistance in Si resistors
Laser assisted oxidation to form $Si0_2$ overlayers
Gettering of wafers

Despite these limitations, it appears that laser annealing may soon find industrial application in the fabrication of semiconductor devices. Annealing with pulsed lasers occurs when the ion-implanted layer is heated to the melting point. Recrystallization proceeds via liquid-phase epitaxial regrowth from the substrate with almost 100% of dopant atoms subsequently occupying substitutional sites. This is accompanied by some redistribution of the dopant.

2.5.1. Annealing - CW Lasers

CW annealing of semiconductors occurs through solid-phase epitaxial regrowth. This is similar to the process occurring during thermal annealing in a furnace and does not involve melting. As such, CW annealing maintains dopant distributions and introduces little in the way of surface irregularities. On the other hand, since thermal annealing is an equilibrium process it does not offer the flexibility of pulsed annealing. Furthermore, processing times are lengthened over those characteristic of pulsed annealing. A schematic diagram of a scannable CW annealing system is shown in Figure 2.7. Typical operating conditions are as follows:

Laser power (multiline)	7W
TEM_{oo} spot diameter	38.5 µm
Intensity	6×10^5 W cm^{-2}
x scan speed	2.76 cm S^{-1}

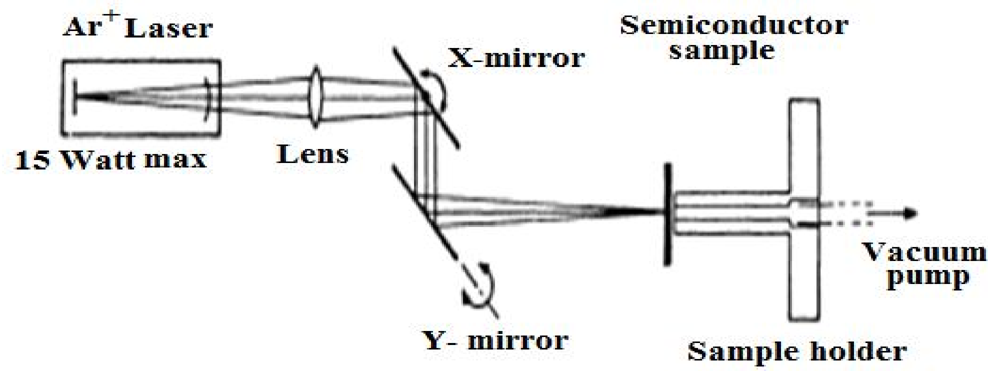

Figure 2.7. System for CW annealing with Ar+ laser.

Under these conditions the width of the annealed line was 22 µm. The y position was changed by ~15 µm at the end of each scan to yield overlapping scans.

Figure 2.8 shows a comparison between As concentration profiles and Si subjected to a 30-min, 1000 ^{O}C thermal anneal and that obtained after CW laser annealing. This plot shows that the As distribution is essentially unaffected by CW laser annealing while thermal annealing leads to significant redistribution. In addition, a fairly sharp boundary is produced between recrystallized and amorphous zones. This boundary can be seen in the electron micrograph of laser scanned B:Si shown in Figure 2.9. CW laser annealing provides complete recrystallization with 100% electrical activity (W. W. Du'ley 1983). This is observed for both amorphous and nonamorphous surface implants on Si.

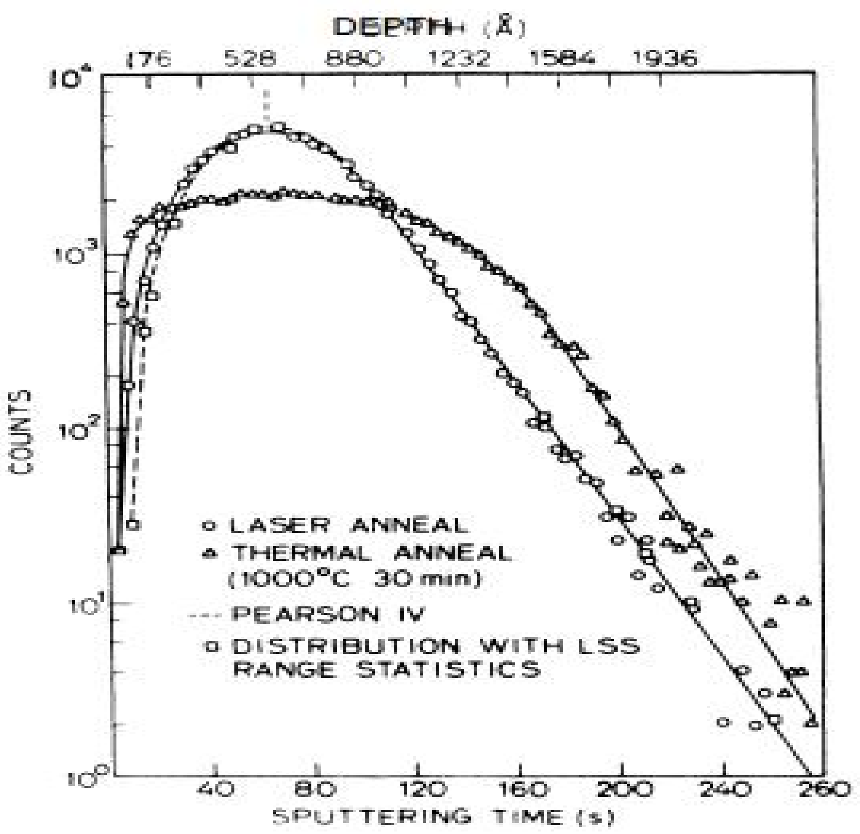

Figure 2.8. As concentration profile in As-implanted Si after laser anneal and thermal anneal.

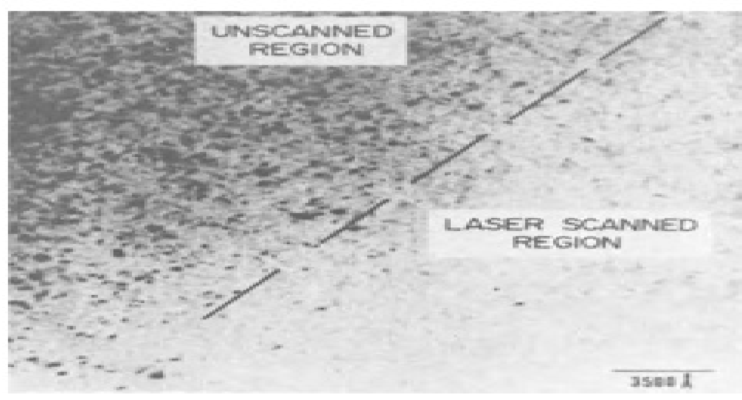

Figure 2.9. Transmission electron micrograph of B-implanted laser annealed sample at laser scan boundary (W. W. Du'ley 1983).

Two other general investigations of CW annealing of As implanted Si have been reported, (W. W. Du'ley 1983). Both groups conclude that CW annealing is consistent with solid-phase epitaxial regrowth. Gat et al. show that the kinetics of this regrowth is compatible with thermal conduction through the sample together with a growth rate.

$$\nu = 1.55 \times 10^{14} e^{-2.3/KBT(r)}$$

where v is the growth rate in A S^{-I}, KB the Boltzmann constant (8.6 X 10^{-5} eV $K)^{-I}$, and T(r) the temperature at radial distance r from the center of the focused beam.

Since the band gap of Si is 1.1 eV, CO_2 laser radiation *(hv* = 0.12 eV) is not strongly absorbed. However, absorption does occur via free carriers and transitions to and from impurity levels. Celler *et af.* (1979) have studied the CW annealing of ion-implanted Si with CO_2 and CW Nd-YAG lasers. In view of the weak absorption at both laser wavelengths, it was found that preheating of substrates to 200-400 ^{O}C was advantageous. Since the absorption coefficient is small, heating occurs over a larger volume than with Ar or Kr lasers. Electrical activity was smaller than that obtained with Ar or Kr annealing. CO_2 or Nd-YAG laser annealing therefore appears to offer a capability that is intermediate between that of CW Ar and thermal annealing. CW annealing with a CO_2 laser has been used in the preparation of nitrogen

isoelectronic traps in $GaAs_{0.6}$ $P_{0.4}$ light emitting diodes . The conversion efficiency of GaAs solar cells has been improved by annealing with CW Nd-YAG laser (W. W. Du'ley 1983).

2.5.2. Recrystallization

While much effort has been devoted to the development of laser-annealing techniques for epitaxial regrowth of ion-implanted amorphous layers on semiconductors, similar methods can be used for the production of large grained semiconductor sheets.

Recrystallization of 0.4μm thick polycrystalline films of chemically vapor deposited Si that had been implanted with B using a CW Ar^+ system (W. W. Du'ley 1983). A summary of their data is given in Table 2.3. It can be seen that laser annealing leads to a dramatic increase in grain size and raises carrier concentration to the limit provided by implantation ($\approx 5 \times 10^{14}$ B^+ cm^{-2}). Carrier mobilities exceeded those obtained with thermal annealing.

Table 2.3. Electrical Properties and Structure Comparison of Different Laser Anneal Condition on 5 X 10^{14} B^+ cm^{-2} Implanted Polysilicon.

Anneal condition	As-implanted	Thermal anneal	Laser Anneal	Laser after thermal Anneal
Grain size	300 - 600 Å	900-1200 Å	$\overline{25} \times \overline{2}\ \mu m$	$\overline{25} \times \overline{2}\ \mu m$
Sheet resistivity $\Omega\square^{-1}$	12.5 M	623	269	260
Sheet carrier concentration (cm^{-2})	Unmeasurable	4.7 X 10^{14} cm^2	5.2 X 10^{14} cm^2	5.17 X 10^{14} cm^2
Mobility (cm^2 V^{-1} S^{-1})	Unmeasurable	24	44.5	46

Recrystallization of Ge films on Si substrates with a CW Nd-YAG laser focused to a slit image yields the structure shown in Figure 2.10. The spatial

period of this structure was found to be a sensitive function of substrate temperature ranging from ≈ 50 μm at 20 °C to 250 μm at 475 °C. As shown in the inset of the figure, the crystal structure varies within each period from amorphous to mixed amorphous-crystalline to a region of larger crystallites (W. W. Du'ley 1983).

Irradiation of Ge films on Mo or graphite substrates heated to 400 - 500 °C over a localized region was found to initiate recrystallization over areas as large as 2.5 X 2.5 cm^2. It is possible that this process may lead to a competitive method of forming single-crystal sheets of semiconductor material for use in the manufacture of solar cells (W. W. Du'ley 1983).

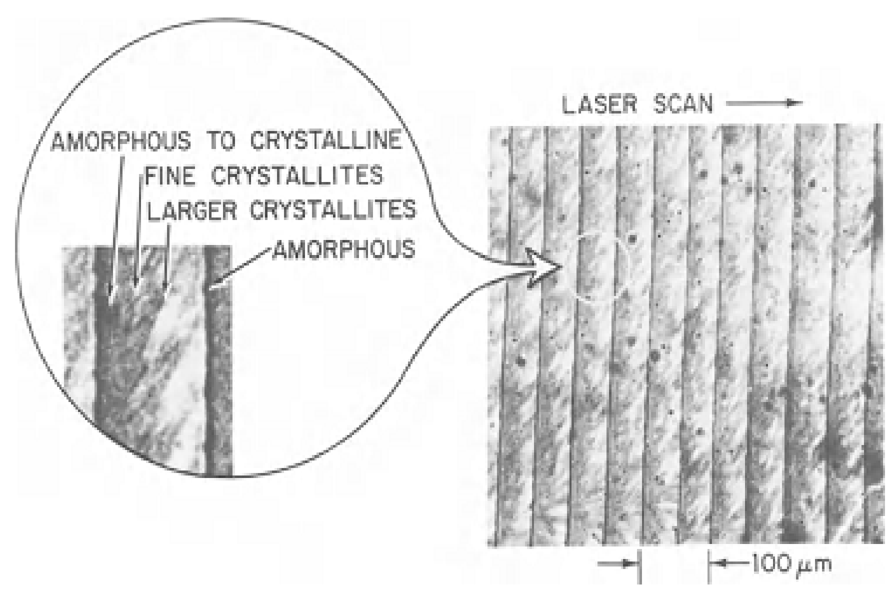

Figure 2.10. Optical transmission micrograph of a laser crystallized Ge film showing periodic structural features. Inset: expanded view illustrating four different microstructure regions.

2.5.3. Laser induced formation of silicide

Device performance necessitates scaling of device feature size and the tailoring of silicide contact formation becomes critical with limiting thermal budget. Laser thermal processing of silicides has been first done by melting thin silicide layers by Q-switch Nd-YAG laser melting of Ni,

Pd, or Pt film on Si. Laser induced interaction between various types of metal such as Au, Pt, Pd, Ti, Co, Mo, Ni and W with Si have since been reported (J. Lawrence, J. Pou, D. K. Y. Low, and E. Toyserkani 2010). These prior works established the fundamental understanding of the formation of metal silicon compounds using laser irradiation. It was found that the formation of cellular structure in the solidifying phase was attributed to the supercooling and convection in the melt during the solidifiation process. The possibility of amorphous phase formation found in the Pt-Si and Pd-Si has been correlated to the composition of the melt. Another promising result has reported the formation of low resistivity (150–300 μΩcm) WSi_2 through pulsed laser irradiation in vacuum environment while laser anneal in an N_2 atmosphere serves to accelerate the silicidation reaction during laser annealing process (J. Lawrence, J. Pou, D. K. Y. Low, and E. Toyserkani 2010).

Laser anneal silicide formation was predominantly performed under a high laser fluence (range of 0.7 to 1.5 J/cm^2) in many of the early works (during 1980s). Owing to the energy deposited in the sample, the reaction of thin metal films on Si under such high fluences would usually result in Si-rich silicide phases. When formation of thin silicide layers is required for contact application, it is critical to tailor the laser energy such that it does not induce a very deep Si melt. The rate of solidification during laser annealing process approaching 10^{10} K/s is far from equilibrium. Depending on the fluence, the melt might only last for tens of ns (similar to its laser pulse) before it re-solidifies. Despite having diffusion coefficient of element in liquid in the order of 10^{-4} cm^{-2}/s, melting in such short duration results in non-uniform elemental distribution in the molten film, especially when the thickness of the molten film is much thicker than the diffusion distance of the elements in the melt. During the solidification process of the molten layer, kinetics play an important role as a large undercooling can cause either nucleation or growth to take place.

The effect of laser fluences on different Ni silicide phase formation was demonstrated by Luo et al. in late 1990s (J .S. Luo, W.T. Lin, C. Y. Chang et al. 2000). Lower fluence results in an amorphous overlayer in Ni silicide or germanosilicide whereas cell formation occurred after laser annealing at high laser fluence due to constitutional super cooling. Morphology of the Ni germanosilicide formed on Ni/$Si_{0.76}$ $Ge_{0.24}$ and Ni/Si_{1-x-y} Ge_xC_y has been found to be stabilized with the suppression of agglomeration (J .S. Luo, W.T. Lin, C. Y. Chang et al. 2000). The study of laser annealing time has revealed an enhanced diffusion of the silicide layers based on PtSi formation induced by Nd:YAG pulsed laser annealing (M. C. Li, X.K. Chen, W. Cai et al. 2001). Laser irradiation using Excimer pulsed laser of wavelength 308 nm within 0.2–1.8 J/cm^2 followed by thermal annealing have been used to prepare β-$FeSi_2$ semiconducting silicide. Subsequently, laser annealing has attempted to eliminate the difficulty of Ti silicide transformation from C49 to C54 phase in a narrow structure. The melt depth during Excimer pulsed laser annealing can be controlled using amorphization of Si substrate, which enables the formation of stoichiometric titanium disilicide ($TiSi_2$) with defined silicide depth (G. Verma, S. Talwar and J. C. Bravman 2001). A desired process margin is possible following the melt depth as a function of laser energy at the amorphous Si/crystalline Si interface depth. Using single-pulsed laser annealing, it is possible to form nano-sized grains of C49 phase, which was found to lower the formation temperature of C54 $TiSi_2$ (Y.F. Chong, K. L. Pey, A. T. S. Wee et al. 2001). In a separate work, a C40 $TiSi_2$ template, formed after laser annealing, has been found to facilitate the C54 phase transformation at low temperature RTA without exhibiting any line width dependence (S.Y. Chen, Z. X. Shen, and S. Y. Xu. et al. 2002). Meanwhile, when a bilayer system consists of Ti capped Co films on Si substrate was subjected to pulse laser irradiation, the high concentration of Ti was found to affect the crystallization of the Co silicide and resulted in an amorphous phase formation.

2.6 Literature review

(Bo Lojek 2008), discussed microwave annealing of ion-implanted layers in semiconductors is an emerging application of thermal processing of semiconductors, with low processing temperature eliminating unwanted diffusion as the main potential advantage. Requirements and limitations of the microwave processing chamber are discussed first, and secondly, for the first time, results from a processed manufacturing lot using microwave annealing are discussed. The achieved results show that is feasible to achieve the same level of activation of implanted layers as in conventional high temperature RTP processing using the microwave at temperatures below 400 ^{o}C, and equivalent processing time.

(Miin-Horng Juang, C.N. Lu , S.L. Jang et al. 2010), reported on formation of excellent ultra-shallow p+ n junctions by thermally treating the BF_2^+-implanted Si samples by excimer laser annealing (ELA) at 300- 400 mJ cm^{-2} with post low-temperature long-time furnace annealing (FA) at 600 ◦C. A junction with a leakage current density lower than 20 nA cm^{-2} and a sheet resistance smaller than 200Ω □$^{-1}$ can be well achieved. No considerable dopant diffusion is observed by using this low-thermal-budget annealing process. However, by simply using the ELA treatment at 300–400 mJ cm^{-2}, the resultant junction shows a leakage current density as high as 10^4 nA cm^{-2} and a peripheral leakage current density of 10^3 nA cm^{-1} . The large junction leakage is primarily due to the leakage current generated within the junction region near the local-oxidation-of-silicon (LOCOS) edge, and which is substantially caused by the ELA treatment. The large peripheral junction leakage current density can be significantly reduced to be about 0.2 nA cm^{-1} after a post low-temperature FA treatment at 600 ◦C. As a result, the scheme that employs ELA treatment with post low-temperature furnace annealing treatment would be efficient for forming excellent ultra-shallow p+n junctions at low thermal budget.

$(Ba,Sr)TiO_3$ Barium Strontium Titanate (BST) thin film with a perovskite structure has a potential for the practical applications in various functional devices. Normally, the BST thin films derived from solegel and sputtering are amorphous or partially crystalline when processed below 700 ^{O}C. For the purpose of integrating BST thin film directly into system-on-package (SoP), it is necessary to process the BST film below 350 ^{O}C. The electrical properties of low-temperature crystallized BST film studied by (Min Gyu Kang, Kwang Hwan Cho, Seung Min Oh, et. al. 2011). The BST thin films have been crystallized at 300 ^{O}C by excimer laser annealing (ELA). The BST films were exhibited in a single perovskite phase and have well-defined electrical properties such as high dielectric constant, low dielectric loss and low leakage current density. As a result, we demonstrated crystallized BST thin film which has permittivity of 143, dielectric loss of 0.028 and leakage current density of 0.9 mA/cm^2 below 300 ^{O}C.

A new anode/cathode design and process concept for thin wafer based silicon devices is proposed to achieve the goal of providing improved control for activating the injecting layer and forming a good ohmic contact was discussed by (M. Rahimo, J. Vobecký, C. Corvasce et al. 2012). The concept is based on laser annealing in a melting regime of a p-type anode layer covered with a thin titanium layer with high melting temperature and high laser light absorption. The improved activation control of a boron anode layer is demonstrated on the soft punch through Insulated Gate Bipolar Transistor (IGBT) with a nominal breakdown voltage of 1700 V. Furthermore, the silicidation of the titanium absorbing layer, which is necessary for achieving a low $V_{CE\ ON}$, is discussed in terms of optimization of the device electrical parameters.

(Zhanyong Wang, Hongyang Zhao, Qiwen Yao et. al. 2013) reported a ZnO/Co multilayers with different layers that have been deposited on silicate (100) substrate by the pulsed laser deposition method. The as-deposited

multilayers present the structure of amorphous phase and a narrow hysteresis loop with high saturation magnetization and low coercivity, showing the typical soft magnetic behavior. The post annealing at the elevated temperature causes the transformation from as-deposited amorphous phase to crystalline metallic cobalt and ZnO phase, as well as the interdiffusion of different layer forming CoO and $ZnCo_2O_4$ phases. The presence of crystalline metallic cobalt phase with ferromagnetic (FM) and cobalt oxide (CoO) phase with antiferromagnetic (AFM) is beneficial to the FM–AFM coupling, resulting in the shift of widening of the hysteresis loop. But an excessively high annealing temperatures leads to the formation of large amount of simple or complex oxides with paramagnetic, antiferromagnetic properties, inducing the decrease of magnetic properties significantly.

(Romain Beal , Khalid Moumanis, Vincent Aimez, et. al. 2013) reported the fabrication of superluminescent diodes (SLD) from a graded bandgap quantum well intermixed (QWI) material obtained by an infrared laser rapid thermal annealing (IR Laser-RTA) technique. The processed semiconductor wafer consisted of an InGaAs/InGaAsP/InP (001) QW laser heterostructure originally emitting at 1.55 μm. The combined beams of a 150 W laser diode operating at 980 nm and a 30 W Nd:YAG laser operating at 1064 nm are used to heat the sample. While the laser diode is used for back-side heating of the wafer, the Nd:YAG laser beam is swept along the sample surface, resulting in temperature gradient changing in the direction perpendicular to the scan. This contactless RTA approach, allowed to obtain a graded bandgap material that was employed for the fabrication of SLD devices with a broadened emission bandwidth. The lasing effect in a series of 3 mm long broad area injection diodes was suppressed by tilting their facets by 7.51 with respect to the [110] direction. The best SLD devices had their FWHM (full-width-at-half-maximum) emission increased by 33% in comparison to the FWHM of 36 nm observed for devices made from the as grown material at an equal output power of 0.8 mW.

(Chien-Yie Tsay and Tzu-Teng Huang 2014), employed KrF excimer laser annealing (ELA) treatment on sol–gel derived indium–zinc oxide (IZO) precursor films to develop a method of low thermal-budget processing. As-coated IZO sol–gel film was dried at 150 ^{o}C and then annealed using KrF excimer laser irradiation under ambient air. The laser irradiation energy density was adjusted to 150, 250, 350, and 450 mJ/cm^2 to investigate the effects of laser irradiation energy density on the microstructure, surface morphology, optical transmittance, and electrical properties of laser annealed IZO thin films. Results of Grazing Incidence X-ray Diffraction GIXRD and Transmission Electron Microscope -Selected Area Electron Diffraction (TEM-SAED) indicated that the ELA IZO thin films had an amorphous phase structure. The surface characteristics and electrical properties of laser annealed IZO thin films were significantly affected by the laser irradiation energy density. It was found that the dried IZO sol–gel films irradiated with a laser energy density of 350 mJ/cm2 exhibited the flattest surface, the highest average optical transmittance in the visible region, and the best electrical properties among all ELA samples.

$Ni_{1-x}Mg_xO$ thin films for Metal–Semiconductor–Metal (MSM) ultraviolet (UV) photodetector were deposited by pulsed laser deposition. The effects of rapid thermal annealing (RTA) on both structural and optical properties of the thin films were studied by (Yanmin Guo , Liping Zhu, Jie Jiang et. al. 2014). After RTA treatment, the $Ni_{1-x}Mg_xO$ films showed better crystalline quality with a larger optical band gap. Moreover, the effect of RTA on the current–voltage characteristics of MSM UV photodetector fabricated on the $Ni_{1-x}Mg_xO$ thin film was investigated, too. The results revealed that the series of dark current is significantly reduced from 390.50 nA (as-deposited) to 19.96 nA (RTA treated at 1000 °C), which can lead to higher signal-to-noise ratio of the photodetector. Thus the performance of the photodetector was enhanced by RTA to the Ni1 – xMgxO thin films.

(Chen Wang, Cheng Li, Shihao Huang et al. 2014), focused their study on phosphorus diffusion in ion-implanted germanium after excimer laser annealing (ELA). An analytical model of laser annealing process was developed to predict the temperature profile and the melted depth in Ge. Based on the heat calculation of ELA, a phosphorus diffusion model has been proposed to predict the dopant profiles in Ge after ELA and fit SIMS profiles perfectly. A comparison between the current–voltage characteristics of Ge n^+/p junctions formed by ELA at 250 mJ/cm^2 and rapid thermal annealing at 650 ^oC for 15 s has been made, suggesting that ELA is promising for high performance Ge n^+/p junctions.

(C. Charpentier, R. Boukhicha , P. Prod'homme et al. 2014), examined in detail the evolution of the properties of room-temperature sputtered ZnO:Al thin films during process of the use of a combined excimer (XeCl = 308 nm) laser annealing (ELA) and chemical etching process (dubbed the "LaText" process) to generate textured ZnO:Al thin films suitable for thin-film silicon photovoltaic applications. They revealed (i) the bulk structural changes induced during laser annealing through X-ray diffraction measurements (XRD) and Raman spectroscopy, (ii) the dramatic changes in surface morphology and macroscopic electronic properties before and after each step of the LaText process, through Atomic Force Microscopy (AFM), Scanning Electron Microscopy (SEM) and Hall effect measurements, and (iii) the exceptional light scattering properties of these films in both air and in a cell configuration, as measured by optical transmission and reflection measurements. In all, they showed that the electronic transport properties in the final state are acceptable for thin film PV applications, and the optical properties are exceptional and demonstrate great potential for light-trapping performance for both a-Si:H and μc-Si:H solar cells.

(Taj Muhammad Khan M. Zakria, Mushtaq Ahmad et. al. 2014) described and investigated the stability of the room temperature ZnSe thin films with thermal annealing deposited onto glass by pulsed laser deposition technique

using third harmonic 355 nm of Nd: YAG laser beam. Optoelectronic analysis and stability with thermal annealing was described in terms of structural and optical properties. These properties were investigated via X-ray diffraction, atomic force microscope, scanning electron microscope, Raman, Fourier transform infrared and photoluminescence spectroscopies. From the strong reflection corresponding to the (111) plane ($2\theta = 27.48^o$) and the longitudinal optical "LO" phonon modes at 250 cm^{-1} and 500 cm^{-1} in the X-ray diffraction and Raman spectra, a polycrystalline zincblende structure of the film was established. At 300 and 350 ^oC annealing temperatures, the film crystallites were preferentially oriented with the (111) plane parallel to the substrate and became amorphous at 400 ^oC. Atomic force microscopic images showed that the morphologies of ZnSe films became smooth with root mean squared roughness 9.86 nm after annealing at 300 and 350 ^oC while a rougher surface was observed for the amorphous film at 400 ^oC. Fourier transform infrared study illustrated the chemical nature and Zn–Se bonding in the deposited films. For the as-deposited and annealed samples at 300 and 350 ^oC, scanning electron micrographs revealed mono-dispersed indistinguishable ZnSe grains and smooth morphological structure which changed to a cracking and bumpy surface after annealing at 400 ^oC. The physical phenomenon of annealing induced morphological changes could be explained in terms of "structure zone model". Excitonic emission at 456 nm was observed for both as-deposited and annealed film at 350 ^oC The transmission spectrum showed oscillatory behavior because of the thin film interference and exhibited a high degree of transparency down to a wavelength of 500 nm. Energy band-gap was increased from 2.65 eV to 2.7 eV for the annealed crystalline film at 350^oC which was further decreased to 2.56 eV for the annealed amorphous film at 400^oC. The observed results manifested that room temperature pulsed laser ablated ZnSe thin film showed excellent structural, optical and morphological stability up to 350 ^oC for optoelectronic applications.

(S.A. Moshkalev V.A. Ermakov , A.R. Vaz et. al. 2014) presented a new approach for electrical and thermal improvement of contacts between carbon nanostructures (multi-wall carbon nanotubes – MWCNTs and multi-layer graphene – MLG) and metal electrodes by localized laser heating. The nanostructures were deposited over electrodes using the dielectrophoresis (DEP) technique. A focused laser beam was used for direct heating of the samples in ambient atmosphere. The Raman spectroscopy was used to determine the process temperature by observations of the graphitic G-line downshift. In the laser annealing experiments, the G-line position was found first to downshift linearly with laser power indicating gradual heating of the sample proportional to the absorbed power. However, with increasing power the shift was found to saturate at levels that depend on the metal and the contact area. This saturation was attributed to gradual increase of the contact area and improvement of the thermal contacts between the nanostructures and metal electrode that can occur during sample heating. The maximum sample temperature in the beginning of the annealing process was always higher for MLG samples, due to smaller area of contact established between rigid multi-layer graphene and initially rough metal surface. The final result is the increased heat losses to the electrodes and, subsequently, the reduction of the samples temperature. The main advantage of this method, when compared with traditional and rapid thermal annealing, is that the thermal treatment is localized in a small pre-determined region, allowing individually controlled annealing process.

CHAPTER THREE

Materials and Methods

3.1 Introduction

In this chapter, a detailed description of the experimental work, the lasers used in the treatment of samples and the instruments that were used to investigate the samples after irradiated are presented. The experimental procedure is illustrated also in this chapter.

3.2 Materials

The samples used in this work are silicon diodes with specifications listed in table 3.1. These samples were divided into four groups; First one was three samples irradiated by Q- switched Nd:YAG laser (1064nm), the pulse energy of this laser was 1000 mj with repetition rate of 3, 4 and 5 Hz, respectively.

Table (3.1). Silicon diode parameters.

Parameters	Symbol	Maximum Rating	Unit
Maximum repetitive peak reverse voltage	V_{RRM}	50	V
Maximum RMS voltage	V_{RMS}	35	V
Maximum DC blocking voltage	V_{DC}	50	V

The second group was four samples, irradiated by Q- switched Nd:YAG laser (532nm) with pulse energy of (350 mJ, 3 HZ), (300 mJ, 4 Hz), (400 mJ, 3 Hz), and (450 mJ, 4 Hz). The third and fourth groups of the samples composed of 12 silicon diodes, half of the samples were treated by continuous wave CO_2 laser with power of 5, 10, 15, 20, 25, and 30 W, and the other six samples exposed to pulsed CO_2 laser of energy of 500 mJ, 520 mJ, 540 mJ, 560 mJ, 580 mJ, and 600 mJ. The details of these groups are listed in table 3.2. The types and specifications of lasers which were used in this work were presented in table 3.3.

Table (3.2) samples grouping

Group I: the samples which treated by Q-switched Nd: YAG laser (λ=1064 nm)	
The sample	**Laser energy**
Sample (a)	**1000 mJ, 3 HZ**
Sample (b	**1000 mJ, 4 HZ**
Sample (c)	**1000 mJ, 5 HZ**
Group II: the samples which treated by Q-switched Nd: YAG laser (λ=532 nm)	
The sample	**Laser energy**
Sample (a)	**350 mJ, 3 HZ**
Sample (b	**300 mJ, 4 HZ**
Sample (c)	**400 mJ, 3 HZ**
Sample (d)	**450 mJ, 4 HZ**
Group III: the samples which treated by CW CO_2 laser (λ=10.6 µm)	
The sample	**Laser power**
Sample (a)	**5 W**
Sample (b	**10 W**
Sample (c)	**15 W**
Sample (e)	**20 W**
Sample (f)	**25 W**
Sample (g)	**30 W**
Group IV: the samples which treated by pulsed CO_2 laser (λ=10.6 µm) with pulse duration of 0.02 sec.	
The sample	**Laser energy**
Sample (a)	**500 mJ**
Sample (b	**520 mJ**
Sample (c)	**540 mJ**
Sample (e)	**560 mJ**
Sample (f)	**580 mJ**
Sample (g)	**600 mJ**

Table (3.3). Nd:YAG and CO_2 laser types and specifications.

	Nd:YAG	CO_2
Country	China	China
Company	Shanghai Apolo Medical Technology	Beijing Innobri Technology
Model	HS-220E	IB-601B
Laser Type	Q-Switched Nd: YAG	CW + Pulsed
Wavelength	1064 & 532 nm	10600 nm
Pulse Energy	500 & 1000 mJ	600mJ
Pulse Repetition Rate	1Hz, 2Hz, 3Hz, 4Hz, 5Hz	up to 50 Hz
Width of Pulse	<10 ns	<10 ns
Spot Diameter	2-8 mm	
YAG	¢ 7	
Operate Interface	6 "Dual color LCD	
Output power	600W	30 W

3.3 Scanning electron microscope (SEM)

A scanning electron microscope (SEM) is a type of electron microscope that produces images of a sample by scanning it with a focused beam of electrons figure 3.1. The electrons interact with atoms in the sample, producing various signals that can be detected and that contain information about the sample's surface topography and composition.

Figure 3.1 Scanning electron microscope

The electron beam is generally scanned in a raster scanpattern, and the beam's position is combined with the detected signal to produce an image. SEM can achieve resolution better than 1 nanometer. Specimens can be observed in high vacuum, in low vacuum, in dry conditions (in environmental SEM), and at a wide range of cryogenic or elevated temperatures.

3.3.1 Principles and capacities

The types of signals produced by a SEM include secondary electrons (SE), back-scattered electrons (BSE), characteristic X-rays, light (cathodoluminescence) (CL), specimen current and transmitted electrons. Secondary electron detectors are standard equipment in all SEMs, but it is rare that a single machine would have detectors for all possible signals. The signals result from interactions of the electron beam with atoms at or near the surface of the sample. In the most common or standard detection mode, secondary electron imaging or SEI, the SEM can produce very high-resolution images of a sample surface, revealing details less than 1 nm in size. Due to the very narrow electron beam, SEM micrographs have a large depth of field yielding a characteristic three-dimensional appearance useful for understanding the surface structure of a sample. A wide range of magnifications is possible, from about 10 times (about equivalent to that of a powerful hand-lens) to more than 500,000 times, about 250 times the magnification limit of the best light microscopes.

Back-scattered electrons (BSE) are beam electrons that are reflected from the sample by elastic scattering. BSE are often used in analytical SEM along with the spectra made from the characteristic X-rays, because the intensity of the BSE signal is strongly related to the atomic number (Z) of the specimen. BSE images can provide information about the distribution of different elements in the sample. For the same reason, BSE imaging can image colloidal gold immuno-labels of 5 or 10 nm diameter, which would otherwise be difficult or impossible to detect in secondary electron images in biological

specimens. Characteristic X-rays are emitted when the electron beam removes an inner shell electron from the sample, causing a higher-energy electron to fill the shell and release energy. These characteristic X-rays are used to identify the composition and measure the abundance of elements in the sample.

3.3.2 Sample preparation

All samples must be of an appropriate size to fit in the specimen chamber and are generally mounted rigidly on a specimen holder called a specimen stub. Several models of SEM can examine any part of a 6-inch (15 cm) semiconductor wafer, and some can tilt an object of that size to 45°.

For conventional imaging in the SEM, specimens must be electrically conductive, at least at the surface, and electrically grounded to prevent the accumulation of electrostatic charge at the surface. Metal objects require little special preparation for SEM except for cleaning and mounting on a specimen stub. Nonconductive specimens tend to charge when scanned by the electron beam, and especially in secondary electron imaging mode, this causes scanning faults and other image artifacts. They are therefore usually coated with an ultrathin coating of electrically conducting material, deposited on the sample either by low vacuum sputter coating or by high-vacuum evaporation. Conductive materials in current use for specimen coating include gold, gold/palladium alloy, platinum, osmium, iridium,tungsten, chromium, and graphite. Additionally, coating may increase signal/noise ratio for samples of low atomic number (Z). The improvement arises because secondary electron emission for high-Z materials is enhanced.

Nonconducting specimens may be imaged uncoated using environmental SEM (ESEM) or low-voltage mode of SEM operation. Environmental SEM instruments place the specimen in a relatively high-pressure chamber where the working distance is short and the electron optical column is differentially pumped to keep vacuum adequately low at the electron gun. The high-

pressure region around the sample in the ESEM neutralizes charge and provides an amplification of the secondary electron signal. Low-voltage SEM is typically conducted in an FEG-SEM because the field emission guns (FEG) is capable of producing high primary electron brightness and small spot size even at low accelerating potentials. Operating conditions to prevent charging of non-conductive specimens must be adjusted such that the incoming beam current was equal to sum of outcoming secondary and backscattered electrons currents. It usually occurs at accelerating voltages of 0.3–4 kV.

Embedding in a resin with further polishing to a mirror-like finish can be used for both biological and materials specimens when imaging in backscattered electrons or when doing quantitative X-ray microanalysis.

The main preparation techniques are not required in the environmental SEM outlined below, but some biological specimens can benefit from fixation.

3.3.3 SEM Materials

Back scattered electron imaging, quantitative X-ray analysis, and X-ray mapping of specimens often requires that the surfaces be ground and polished to an ultra smooth surface. Specimens that undergo WDS or EDS analysis are often carbon coated. In general, metals are not coated prior to imaging in the SEM because they are conductive and provide their own pathway to ground.

Fractography is the study of fractured surfaces that can be done on a light microscope or commonly, on an SEM. The fractured surface is cut to a suitable size, cleaned of any organic residues, and mounted on a specimen holder for viewing in the SEM.

Integrated circuits may be cut with a focused ion beam (FIB) or other ion beam milling instrument for viewing in the SEM. The SEM in the first case may be incorporated into the FIB.

Metals, geological specimens, and integrated circuits all may also be chemically polished for viewing in the SEM.

Special high-resolution coating techniques are required for high-magnification imaging of inorganic thin films.

3.3.4 Magnification

Magnification in a SEM can be controlled over a range of up to 6 orders of magnitude from about 10 to 500,000 times. Unlike optical and transmission electron microscopes, image magnification in the SEM is not a function of the power of the objective lens. SEMs may have condenser and objective lenses, but their function is to focus the beam to a spot, and not to image the specimen. Provided the electron gun can generate a beam with sufficiently small diameter, a SEM could in principle work entirely without condenser or objective lenses, although it might not be very versatile or achieve very high resolution. In a SEM, as in scanning probe microscopy, magnification results from the ratio of the dimensions of the raster on the specimen and the raster on the display device. Assuming that the display screen has a fixed size, higher magnification results from reducing the size of the raster on the specimen, and vice versa. Magnification is therefore controlled by the current supplied to the x, y scanning coils, or the voltage supplied to the x, y deflector plates, and not by objective lens power.

3.3.5 Beam-injection analysis of semiconductors

The nature of the SEM's probe, energetic electrons, makes it uniquely suited to examining the optical and electronic properties of semiconductor materials. The high-energy electrons from the SEM beam will inject charge carriers into the semiconductor. Thus, beam electrons lose energy by promoting electrons from the valence band into the conduction band, leaving behind holes.

In a direct bandgap material, recombination of these electron-hole pairs will result in cathodoluminescence; if the sample contains an internal electric

field, such as is present at a p-n junction, the SEM beam injection of carriers will cause electron beam induced current (EBIC) to flow.

Cathodoluminescence and EBIC are referred to as "beam-injection" techniques, and are very powerful probes of the optoelectronic behavior of semiconductors, in particular for studying nanoscale features and defects.

3.3.6 Cathodoluminescence

Cathodoluminescence, the emission of light when atoms excited by high-energy electrons return to their ground state, is analogous to UV-induced fluorescence, and some materials such as zinc sulfide and some fluorescent dyes, exhibit both phenomena. Over the last decades, cathodoluminescence was most commonly experienced as the light emission from the inner surface of the cathode ray tube in television sets and computer CRT monitors. In the SEM, CL detectors either collect all light emitted by the specimen or can analyse the wavelengths emitted by the specimen and display an emission spectrum or an image of the distribution of cathodoluminescence emitted by the specimen in real color (Weilie Zhou and Zhong Ling Wang 2006).

3.4 Sputter coating

When a target is bombarded with fast heavy particles, erosion of the target material occurs. The process, when occurring in the conditions of a gaseous glow discharge between an anode and cathode is termed sputtering. Enhancement of this process for scanning electron microscopy (SEM) sample coating is obtained by the choice of a suitable ionization gas and target material. Sputtered metal coatings offer the following benefits for SEM samples:

- Reduced microscope beam damage.
- Increased thermal conduction
- Reduced sample charging (increased conduction).

- Improved secondary electron emission
- Reduced beam penetration with improved edge resolution
- Protects beam sensitive specimens

Increase in electrical conductivity of a sample is probably the single most common requirement for SEM, though all factors come into play with FEG SEM. Low voltage SEM operation can still benefit in many cases from a thin coating (D. E. Newbury, D. C. Joy, P. Echlin, et. al. 1986).

3.5 Samples investigation methods

The samples of group one and group two which were irradiated by the Q-switched Nd: YAG laser with wavelength of 1064 nm and wavelength of 532 nm were placed inside a sputter coater to cover these samples with a thin layer of gold to be prepared for Scanning Electron Microscope (SEM Jeol JXA-840 A, Toyo, Japan). A conductive coating is needed to prevent charging of a sample with an electron beam in conventional Scanning Electron Microscope (SEM) mode (high vacuum, high voltage), and to increase electrical conductivity of a samples. A coating done for these samples in order to take image by SEM to detect the surface defects in the sample treated with furnace annealing, and also to investigate the change in the surfaces of the samples after the treatment with the laser. From current –volt characteristics of the silicon diodes and graphical analysis the dynamic resistance was calculated for each diode before and after laser annealing.

CHATER FOUR

Results and Discussion

4.1 Introduction

A wide variety of physical analytical techniques have been employed in the study of annealed layer structures, and perhaps the most widely used method is Rutherford backscattering and channeling of megaelectron volt ions. However, this does not give direct information about individual crystallographic defects that may be present, and, for this purpose, electron microscopy is unrivaled. Indeed, detailed imaging studies have been indispensable in revealing the varied annealing phenomena characteristic of the solid and liquid phase processes that occur. This chapter relies heavily on the results of scanning electron microscope (SEM) investigations in revealing the microstructural properties of annealed diodes and also this chapter presented on the results obtained from the I-V characteristics curve to study the electrical properties of the samples in terms of the behavior of I-V characteristics and the dynamic resistance of samples irradiated by the lasers.

4.2 Solid phase epitaxial regrowth (SPER)

Solid phase epitaxial regrowth (SPER) is a process whereby amorphised Si is recrystallised upon thermal annealing from temperatures above half that of the melting temperature of the crystal, i.e. for Si from approximately 500 °C, to approximately 1350 °C. The underlying Si crystal acts as a template for the amorphised Si to be arranged upon (epitaxy). This occurs while the Si is still a solid, hence the term solid phase epitaxial regrowth (Matthew Werner 2006).
During SPER the amorphous Si rearranges itself on the underlying crystalline substrate starting from the amorphous/crystalline (a/c) interface and proceeds to the surface in a layer-by-layer fashion. Since crystalline Si has lower free energy there is always a driving force towards rearrangement to the crystal

structure. During SPER, the implanted dopants take up substitutional lattice sites as the crystal-amorphous interface passes through their location. Time resolved reflectivity (TRR) is the main technique that has been used for measuring SPER rates. It has been observed that impurities (dopants) affect the regrowth behavior and the rate of SPER (Matthew Werner 2006).

Figure (4.1) shows the defects on the surface of the silicon diode used in this work. These defects are associated with imperfect regrowth of an amorphous layer and are located in the region of the previously amorphous Si. The main types are hairpin dislocations, microtwins and segregation defects. Hairpin dislocations nucleate when the regrowing a/c interface encounters small microcrystalline regions that are slightly misorientated with respect to the bulk crystalline material. As the microcrystalline pocket is incorporated into the single crystal bulk, a hairpin dislocation is nucleated which propagates to the surface (Matthew Werner 2006 and Chong Yung 2003).

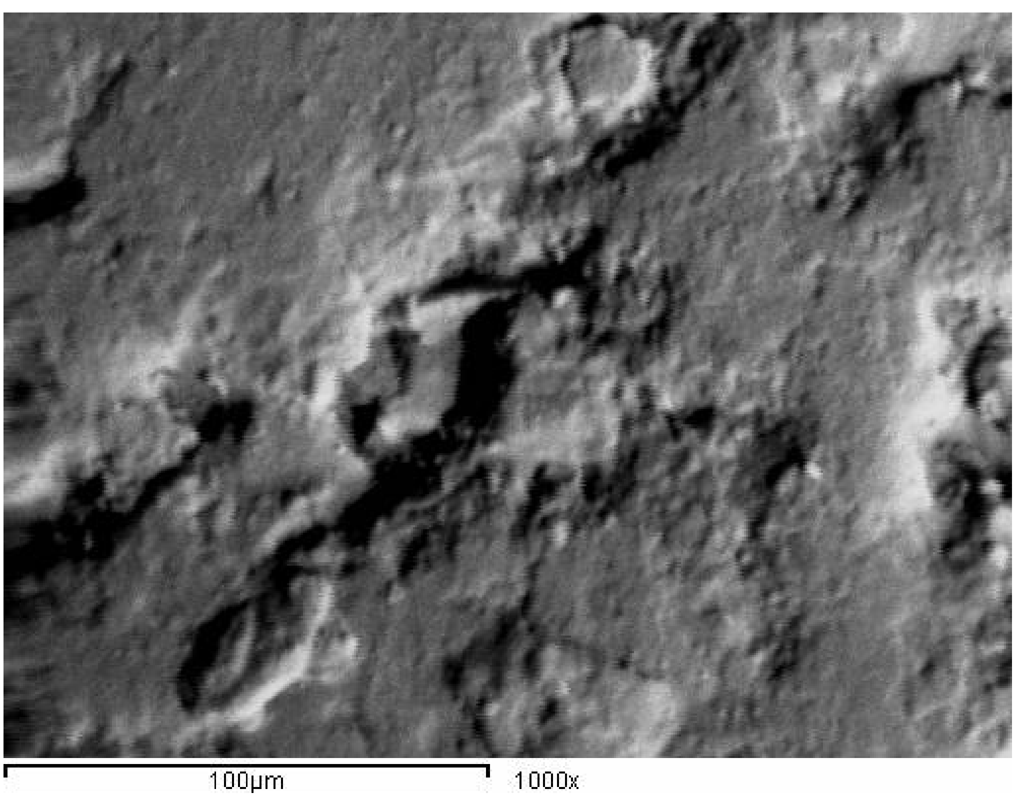

Figure(4.1) Scanning Electron Microscope (SEM) image for the surface of silicon diode after conventional annealing.

4.3-The results of Laser annealing

4.3.1 Annealing by Nd:YAG laser (λ =1064 nm), group I:

Figure (4.2) shows the Scanning Electron Microscope (SEM) photos of silicon diodes subjected to a single-pulse of Nd:YAG laser (1064 nm) with pulse energy of 1000 mj with repetition rate of 3 Hz, in photo (a) , 4 Hz in photo (b), and 5 Hz in photo (c) respectively.

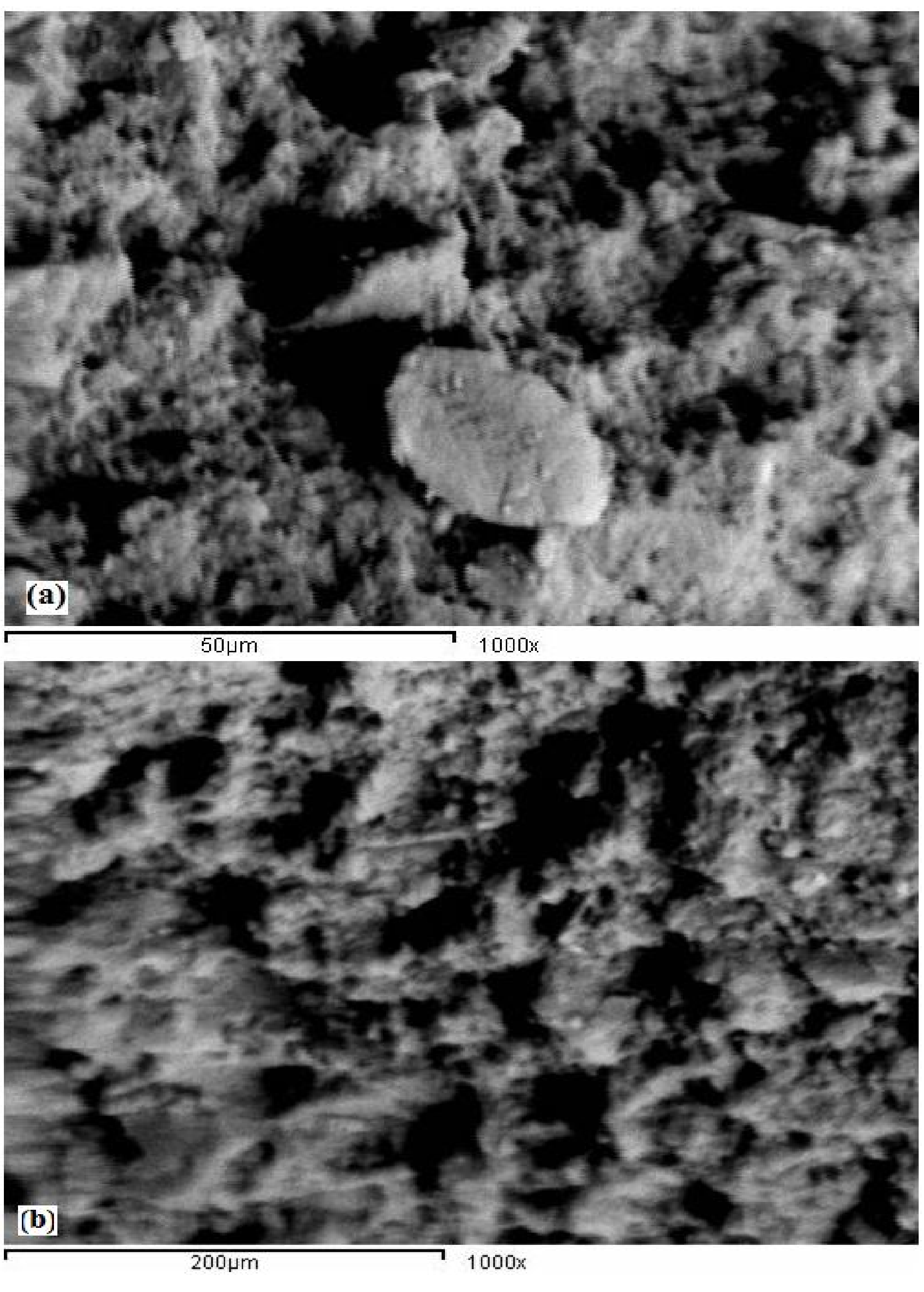

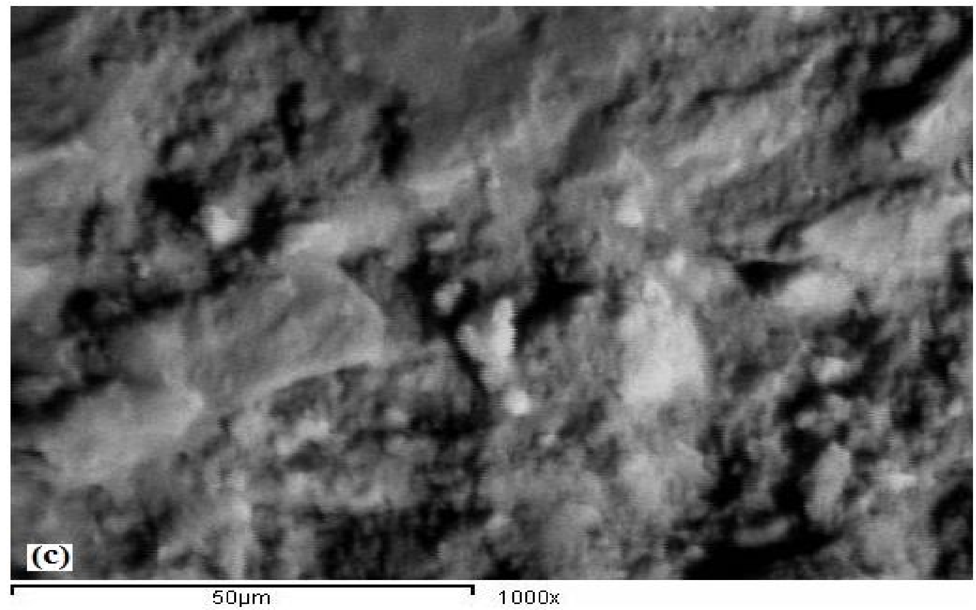

Figure(4.2) Scanning Electron Microscope (SEM) images (a) 1000 mJ, 3Hz (b) 1000mJ, 4Hz (c) 1000mJ, 5Hz.

The change in the dynamic resistance of the diode as a function of the laser repetition rate values for diodes treated with constant pulse energy (1000 mj) and different repetition rate is shown in Figure (4.3), these values are listed in table (4.1). Figure (4.4) shows the room-temperature forward current-voltage characteristics of the diodes, and the values of voltage drop across the diode are listed in table 4.2.

Table (4.1) Dynamic resistance obtained at room temperature for diodes irradiated by Nd:YAG laser (λ=1064 nm).

Repetition Rate (Hz)	Dynamic Resistance (Ω)
0	3.56
3 Hz	3.4
4 Hz	3.11
5Hz	2.64

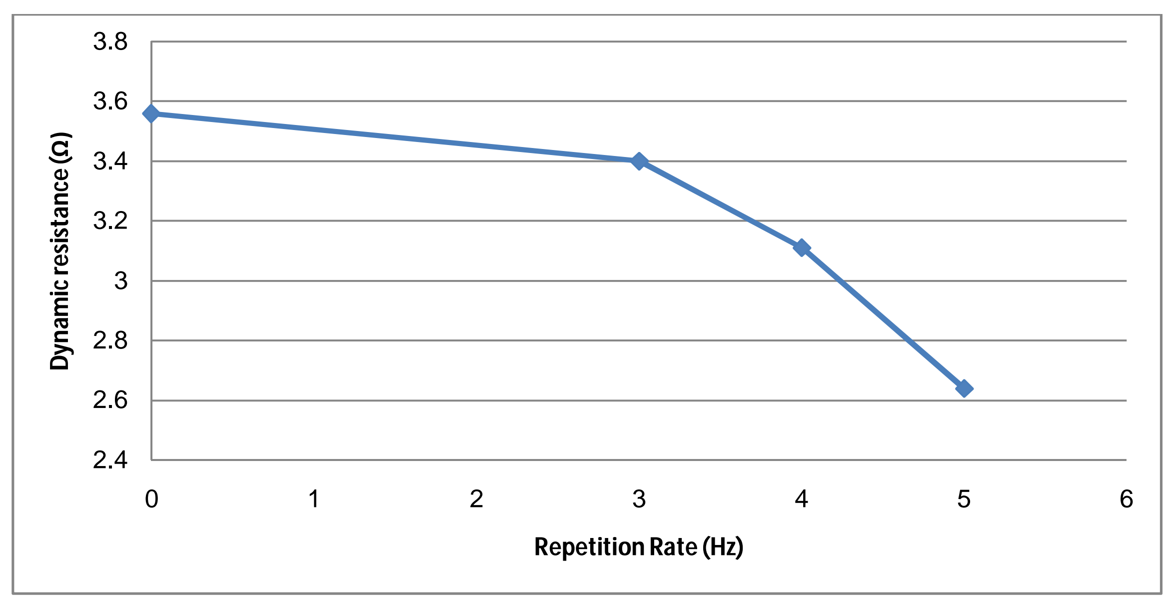

Figure (4.3), the change of dynamic resistance of the diodes with pulse repetition rate

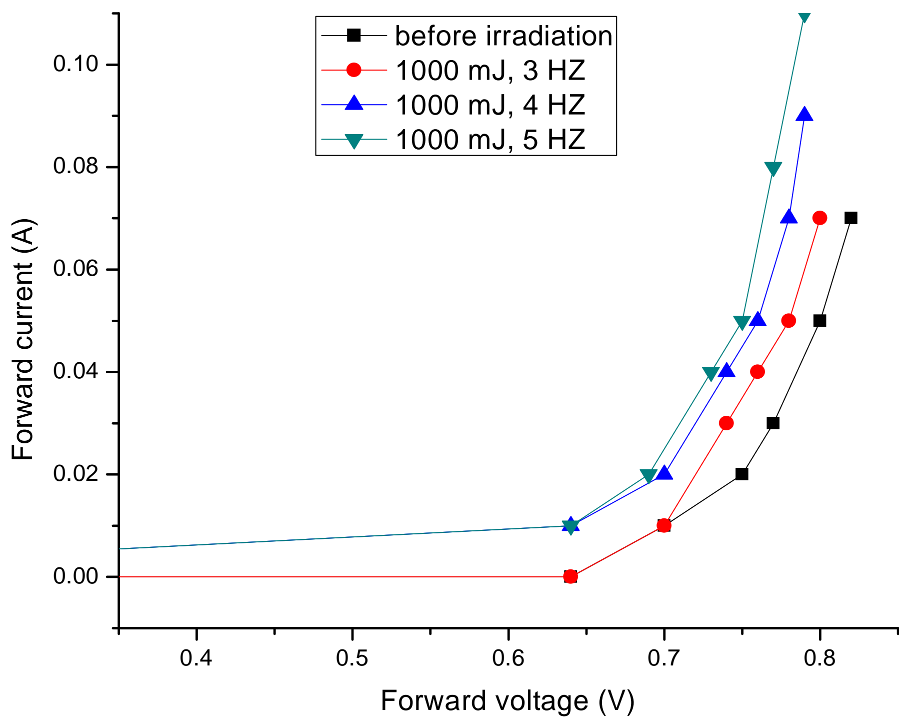

Figure (4.4), I-V characteristics of samples irradiated with pulse energy of 1000 mJ and variable repetition rate by Nd:YAG laser (λ= 1064 nm)

Table (4.2). Data obtained at room temperature for the diodes irradiated by Nd:YAG laser (λ=1064 nm).

Before irradiation		1000 mJ, 3 Hz		1000 mJ, 4 Hz		1000 mJ, 5 Hz	
Volt (V)	Current (A)	Volt (V)	Current (A)	Volt (V)	Current (A)	Volt (V)	Current (A)
0	0	0	0	0	0	0	0
0.64	0	0.64	0	0.64	0.01	0.64	0.01
0.70	0.01	0.7	0.01	0.7	0.02	0.69	0.02
0.75	0.02	0.74	0.03	0.74	0.04	0.73	0.04
0.77	0.03	0.76	0.04	0.76	0.05	0.75	0.05
0.8	0.05	0.78	0.05	0.78	0.07	0.77	0.08
0.82	0.07	0.8	0.07	0.79	0.09	0.79	0.11

4.3.2 Annealing by Nd:YAG laser (λ= 532 nm), group II:

Figure (4.5) shows the scanning electron microscope (SEM) images of the surface of silicon diode after irradiation by Q-switched Nd:Yag laser (λ=532 nm), with pulse energy ranged between 350 mj ,3 Hz, 300 mJ, 4 Hz, 400 mJ, 3Hz, and 450 mj, 4 Hz respectively.

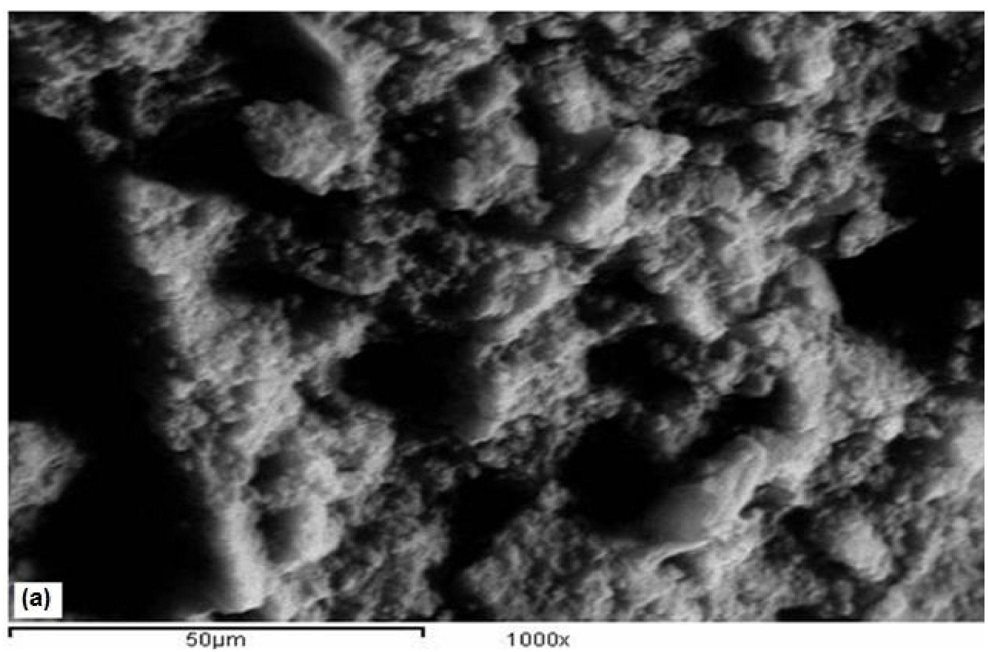

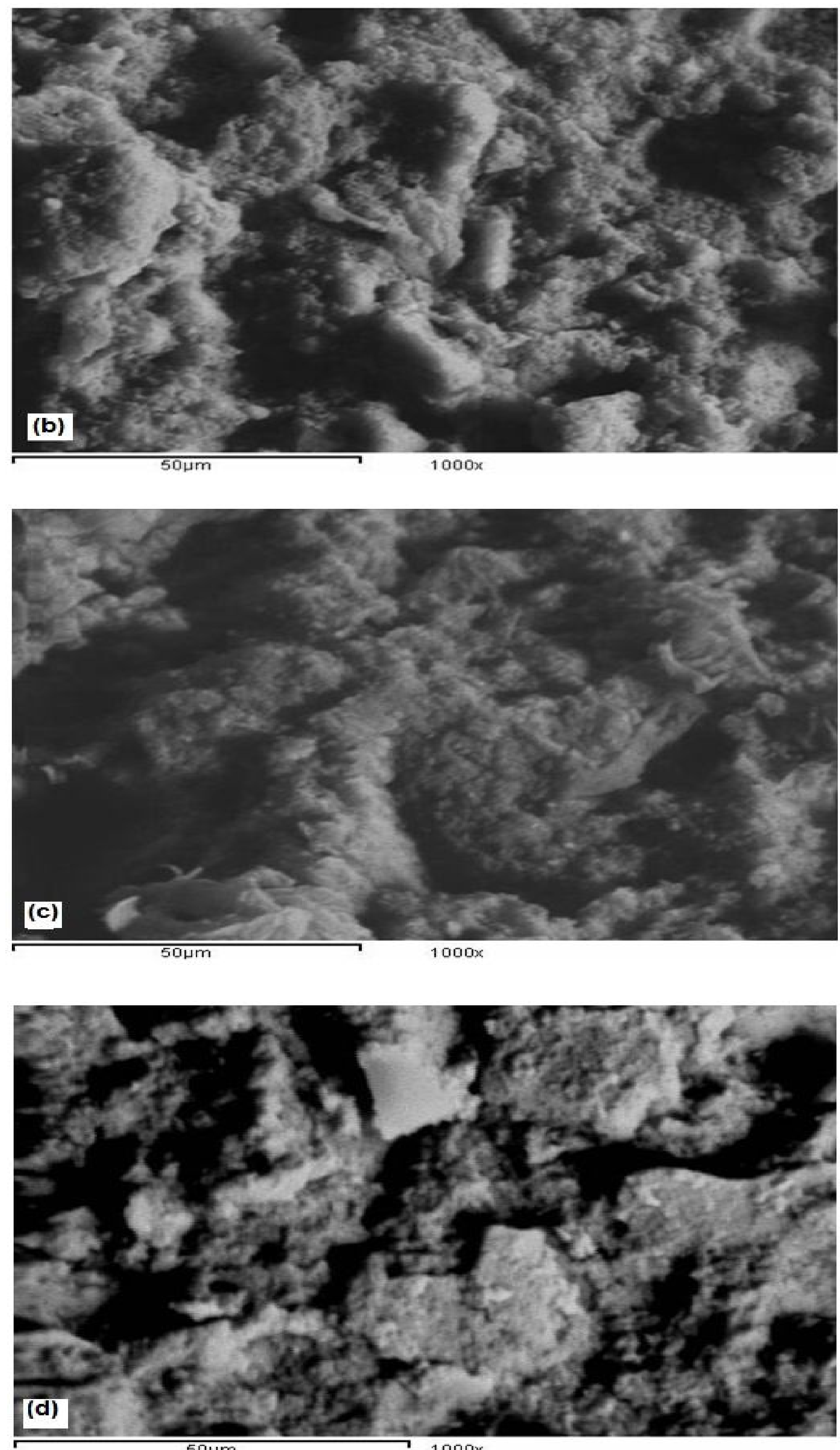

Figure(4.5) Scanning Electron Microscope (SEM) of silicon diodes irradiated by Q-switched Nd:YAG (λ = 532 nm (a) 350 mJ, 3Hz (b) 300 mJ, 4Hz (c) 400 mJ, 3Hz (d) 450 mJ, 4Hz.

Room-temperature forward current-voltage characteristics of the diodes irradiated by the laser and the diode treated by the furnace are shown in figure (4.6), the values of currents passed through each diode and voltage drop across these diodes are listed in table (4.3), the dynamic resistances of all diodes were calculated from the I –V characteristic curve and plotted versus energy dose as shown in figure (4.7).

Table (4.3). Data obtained at room temperature for diodes irradiated by Nd: YAG laser (λ=532 nm).

	Forward Voltage (V)				
Forward current (mA)	Before irradiation	350 mJ, 3Hz	300 mJ, 4 Hz	400 mJ, 3 Hz	450 mJ, 4 Hz
0	0	0	0	0	0
10	0.7	0.7	0.7	0.7	0.7
20	0.736	0.733	0.73	0.725	0.719
30	0.749	0.745	0.745	0.734	0.73
40	0.766	0.762	0.761	0.753	0.745
50	0.774	0.77	0.769	0.762	0.755
60	0.781	0.779	0.775	0.768	0.764
70	0.798	0.794	0.792	0.778	0.775
80	0.817	0.81	0.802	0.792	0.782
90	0.829	0.82	0.816	0.807	0.797
100	0.84	0.829	0.821	0.813	0.808

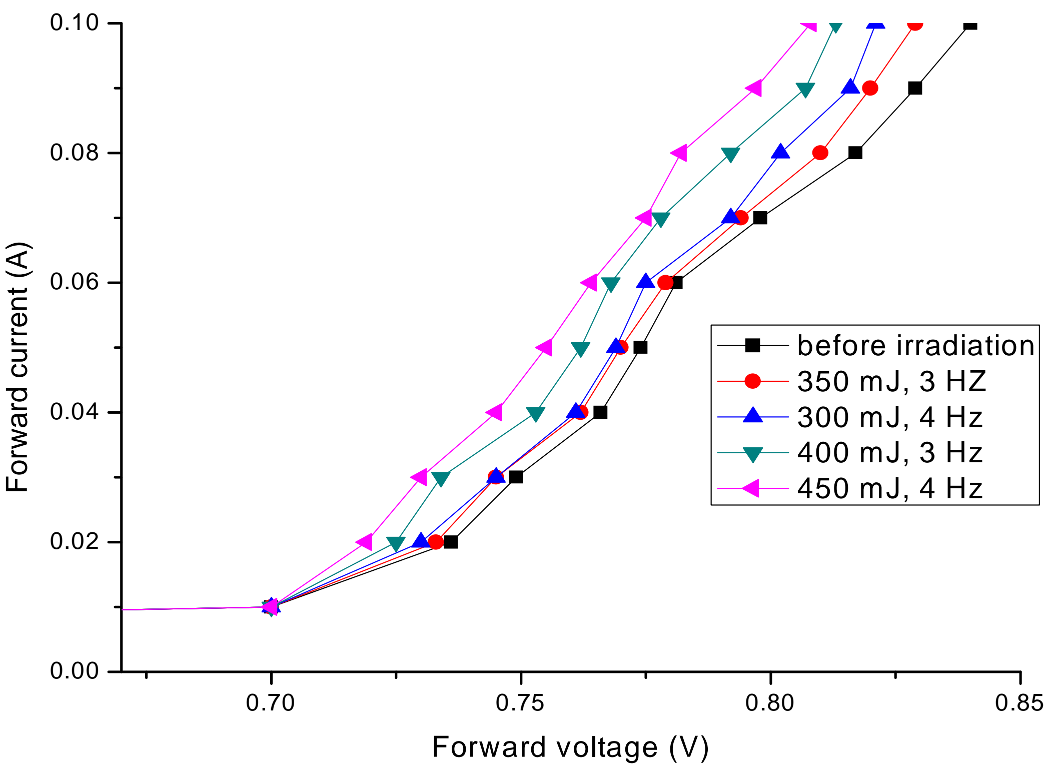

Figure (4.6) I-V characteristics for the diodes irradiated with Nd: YAG/second harmonic generation (λ= 532 nm).

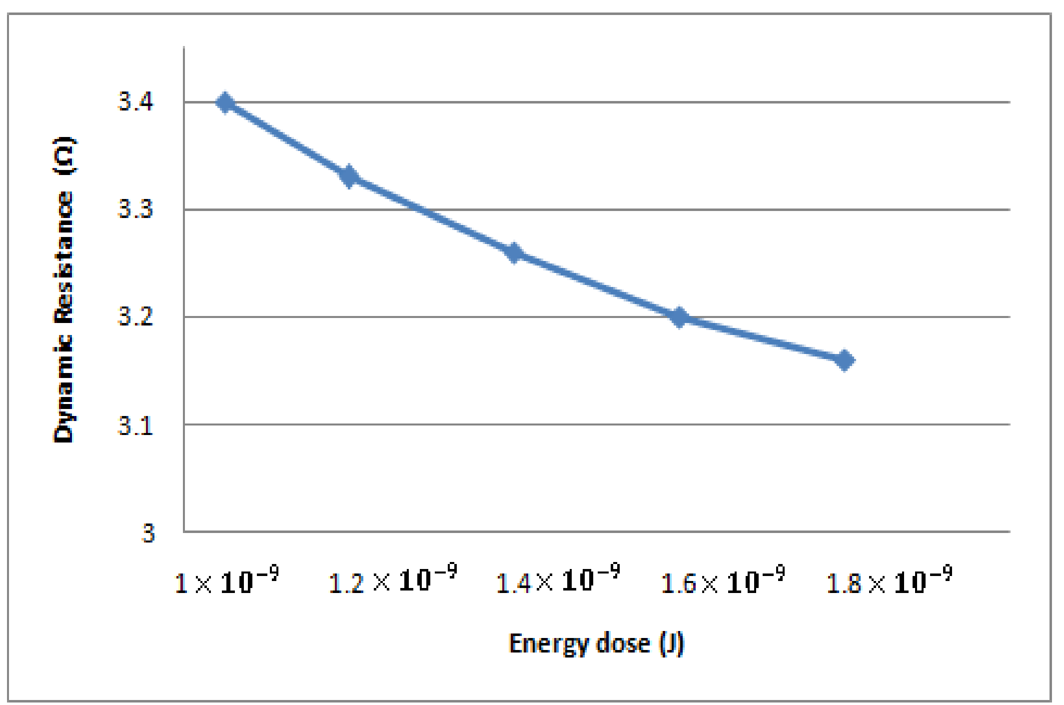

Figure (4.7) the dynamic resistance for the diodes irradiated with Nd: YAG/second harmonic generation (λ= 532 nm).

4.3.3 Annealing by CW CO_2 laser, group III

Figure (4.8) shows the variation in dynamic resistance with respect to laser power values for silicon diodes after annealing by CO_2 at different laser powers ranged from 5 to 30 W and exposure time of 5 seconds for each diode.

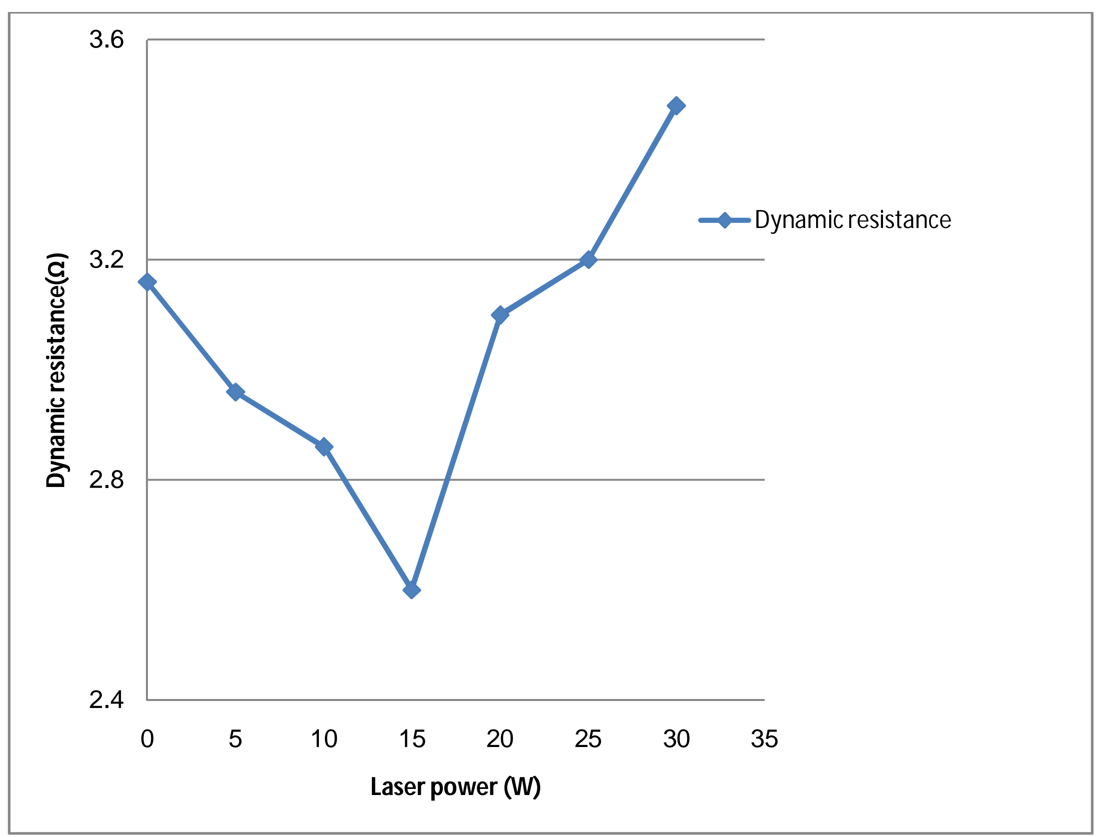

Figure (4.8) the dynamic resistance for the samples irradiated with CW CO_2 laser with different powers.

Table (4.4) lists the room-temperature measurement of current – voltage values for the diode before irradiation and the diodes after irradiation by CW CO_2 laser by different powers of 5, 10, 15, 20, 25 and 30 W, respectively, and the figure (4.9) shows all curves of I-V of all diodes.

Table (4.4). Data obtained at room temperature for diodes irradiated by CW CO_2 laser (10.6 µm).

Forward current (mA)	Forward voltage (V)						
	Before Irradiation	5 W	10 W	15 W	20 W	25 W	30 W
0	0	0	0	0	0	0	0
10	0.7	0.62	0.61	0.597	0.715	0.718	0.72
20	0.72	0.707	0.7	0.69	0.734	0.74	0.744
30	0.749	0.724	0.72	0.718	0.76	0.75	0.76
40	0.76	0.741	0.737	0.734	0.77	0.76	0.769
50	0.771	0.755	0.747	0.745	0.777	0.77	0.779
60	0.777	0.766	0.754	0.75	0.782	0.777	0.787
70	0.782	0.775	0.761	0.759	0.788	0.783	0.791
80	0.787	0.785	0.771	0.766	0.792	0.79	0.796
90	0.791	0.787	0.78	0.774	0.805	0.81	0.81
100	0.801	0.792	0.788	0.782	0.811	0.815	0.82

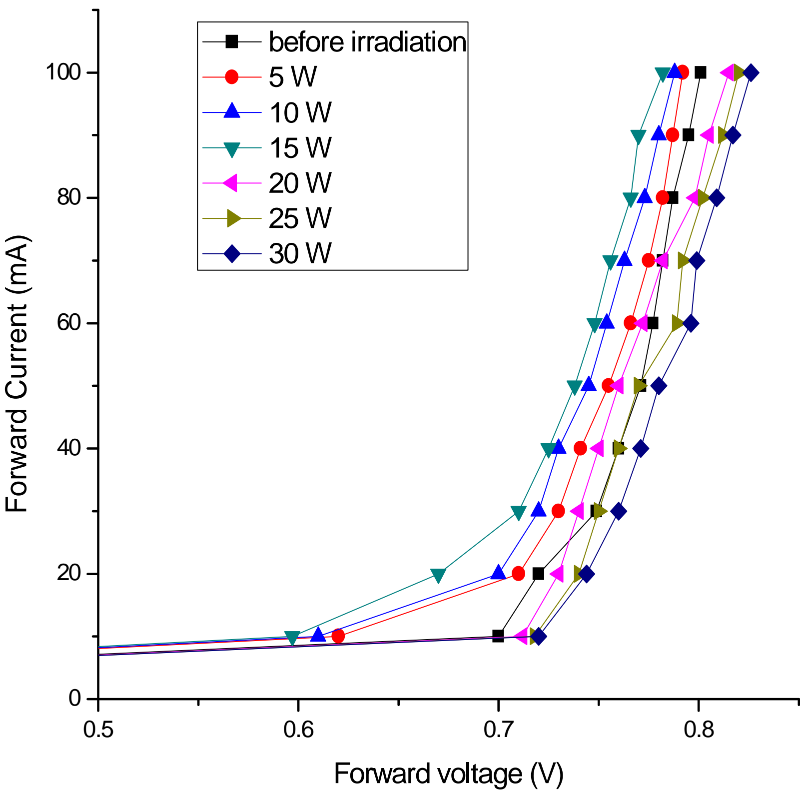

Figure (4.9). Current-voltage characteristics of the diodes treated by different laser powers of CW CO_2 laser.

4.3.4 Annealing by pulsed CO_2 laser, group IV

Figure (4.10) shows the I-V characteristics of the silicon diodes irradiated 5 times for each diode by pulse CO_2 laser with energy ranged from 500 to 600 mJ. The values of voltage drop across each diode corresponding to the its current value were listed in table (4.5), and the relationship between the dynamic resistances which were calculated from I-V characteristics curve for each diode were plotted as seen in figure (4.11).

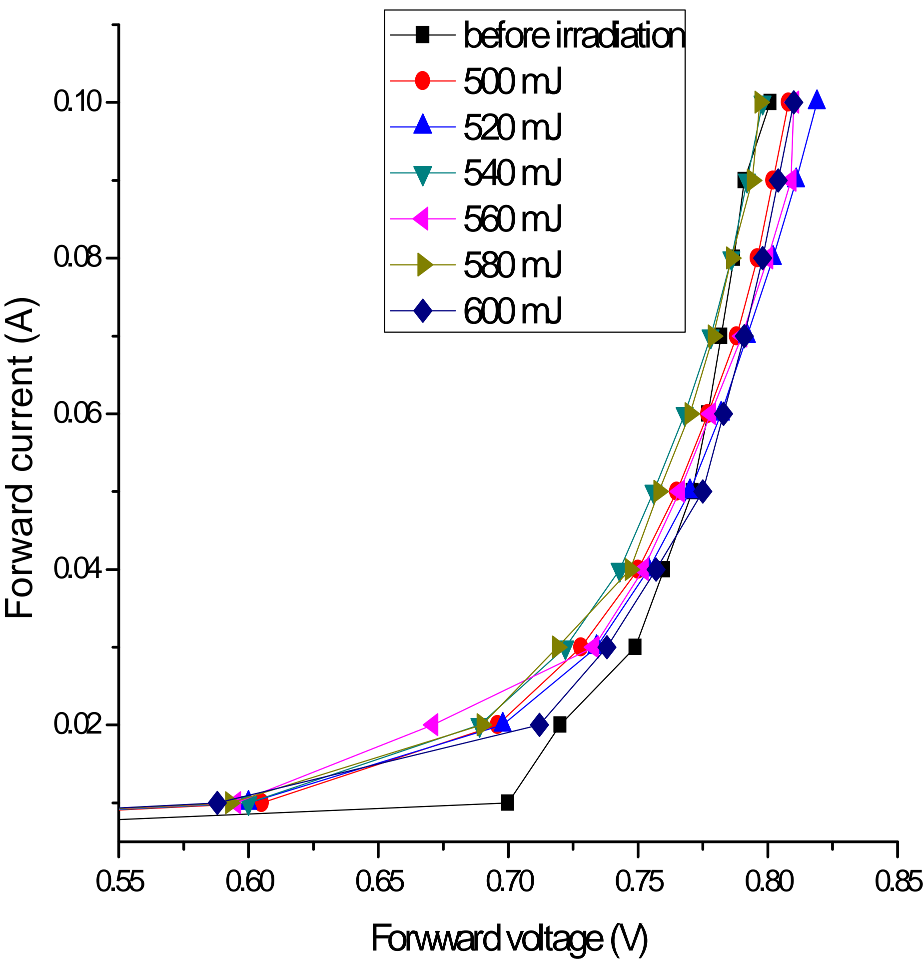

Figure (4.10), I-V characteristics for diodes irradiated by single pulse from CO_2 laser with different energies with pulse duration of 0.02 sec.

Table 4.5 Current- voltage for diodes irradiated by single pulse from pulsed CO_2 laser with different energies.

	Forward voltage (V)						
Forward current (mA)	Before irradiation	500mJ, 50Hz	520mJ, 50Hz	540mJ, 50Hz	560mJ, 50Hz	580mJ, 50Hz	600mJ, 50Hz
0	0	0	0	0	0	0	0
10	0.7	0.605	0.6	0.6	0.595	0.593	0.588
20	0.72	0.696	0.698	0.689	0.671	0.69	0.712
30	0.749	0.728	0.734	0.722	0.733	0.719	0.738
40	0.76	0.75	0.754	0.743	0.752	0.747	0.757
50	0.771	0.765	0.77	0.756	0.766	0.758	0.775
60	0.777	0.777	0.782	0.768	0.778	0.77	0.783
70	0.782	0.788	0.792	0.778	0.79	0.779	0.791
80	0.787	0.796	0.802	0.786	0.8	0.786	0.798
90	0.791	0.802	0.811	0.792	0.809	0.794	0.804
100	0.801	0.808	0.819	0.798	0.81	0.797	0.81

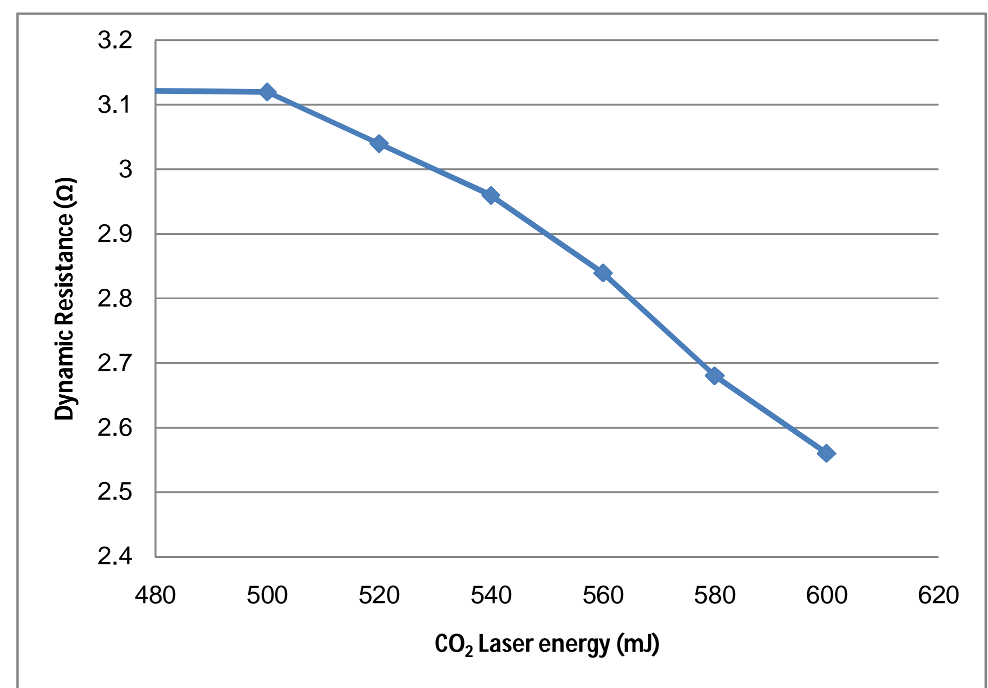

Figure (4.11), the dynamic resistance of the diodes irradiated with single pulse of CO_2 laser with different energies.

4.4 The discussion

4.4.1 Annealing by Nd:YAG laser (λ =1064 nm), group I

From the photos of the Scanning Electron Microscope (SEM), figure (4.2), it can be observed that the surface defects of the diodes are decreased gradually according to the increase in pulse repetition rate (from 3 to 5 Hz). This could be discussed as follows:

In figure (4.2a)**:** the laser energy is only slightly greater than the threshold energy for melting a-Si. In this case, the primary melt (molten layer produced directly by laser irradiation) does not penetrate through the entire a-Si layer. Typically, large-grained (LG) polycrystalline silicon (poly-Si) will be formed near the surface region followed by fine-grained (FG) poly-Si in the underlying region (as illustrated in Figure (4.12b)). The fraction of the LG region increased at the expense of FG region with increasing energy dose – a result of explosive crystallization (J. Lawrence, J. Pou, D. K. Y. Low et al. 2010).

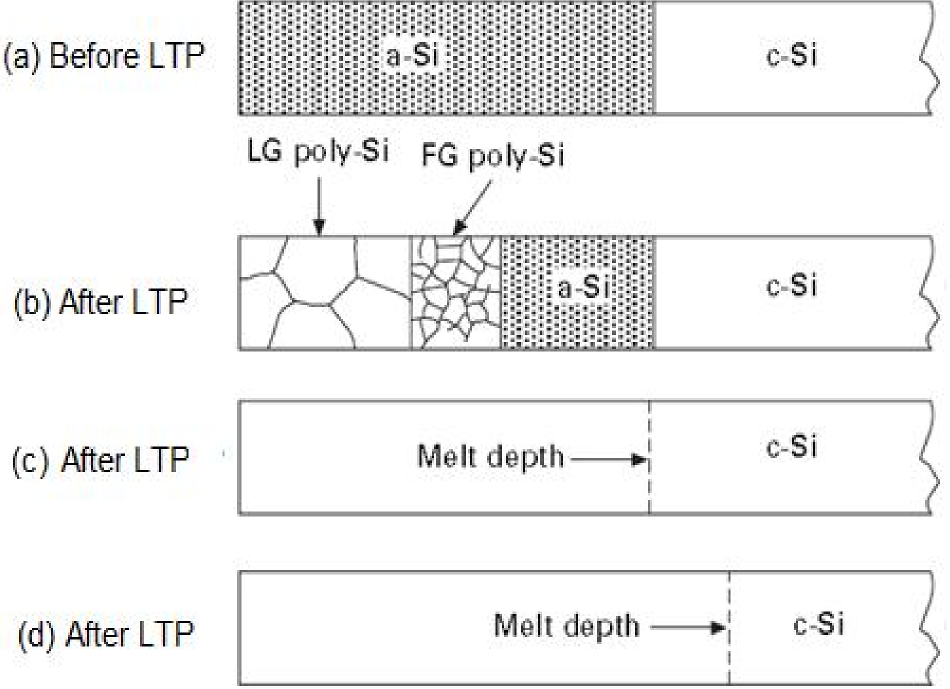

Figure (4.12) Illustration of the structural changes induced by laser irradiation of an a-Si overlayer on c-Si.

Photo (b) in figure (4.2), shows that the laser energy of 1000 mJ with repetition rate of 4 Hz is just sufficient for the primary melt front to reach the a/c interface without melting the underlying c-Si substrate (as illustrated in Figure 4.12c)). Single-crystalline silicon is thus formed via liquid phase epitaxy (LPE), using the underlying substrate as a template (Chong Yung Fu 2003).

In theory, this regrowth process should produce crystals with reasonably good quality, however, it has been reported that residual defects such as microtwins and stacking faults exist in the crystallized layer.

At higher repetition rate, figure (4.2c), the primary melt front penetrates beyond the amorphous/crystalline (a/c) interface (as illustrated in Figure (4.12d)). In this case, single-crystalline silicon is also formed upon solidification. The melting of a part of the crystalline substrate adjacent to the amorphous layer ensures the epitaxial growth of a nearly defectfree crystal with minimum "quenched-in" interstitials (J. Lawrence, J. Pou, D. K. Y. Low et. al. 2010).

The dynamic resistance of the diode before the laser treatment was calculated from the I-V characteristic curve to be 3.56 Ω. As shown in Figure (4.3), a drop in the dynamic resistance from 3.56 Ω to 2.64 Ω is obtained with the increase in the laser repetition rate. This implies that dopant activation has reached a maximum dopant activation upon deep melting of both c-silicon and pre amorphised silicon (PAI) samples, and this can also be attributed to the good current-spreading of top surface layer and a lower contact resistance of anode electrode (J. Lawrence, J. Pou, D. K. Y. Low et al. 2010, J. K. Sheu, J. M. Tsai, S. C. Shei et. al. 2001).

Figure (4.4), shows the room-temperature forward current-voltage characteristics of the samples. From this figure it can be noticed that the diode treated with the furnace and the diode irradiated by 1000 mj with 3Hz repetition rate, exhibit a turn-on voltage of 0.7V at 0.01 A (photo in fig. 4.1 and fig. 4.2a). The two diodes irradiated by 1000 mJ with pulse repetition rate

of 4 and 5 Hz (photo b and c in fig. 4.2), exhibit a turn-on voltage of 0.64 V at 0.01 A. Figure 4.4 and table 4.2 also reveal that the forward voltages is 0.75 at 0.02 A for diode that treated by the furnace, and 0.74 V at 0.03 A, 0.7 V at 0.02 A, and 0.69 V at 0.02 A for the diodes irradiated by 1000 mJ with pulse repetition rate of 3, 4, and 5 Hz respectively. This could be attributed to the improvement in the surface structure and dopant activation when the repetition rate increased above 3 Hz.

4.4.2 Annealing by Nd:YAG laser (λ =532 nm), group II

The photos in figure (4.5), showed clearly that the defects in the surface of the diodes were still present; this is due to the low thermal budget inadequate to reducing defects induced by ion implantation before conventional annealing. Despite that low energy is insufficient to reduce defects, but there is a slight improvement in the I-V characteristics of silicon diode as shown in figure (4-6). This improvement is due to the good absorbance of the surface of the silicon diode to the wavelength of 532 nm, and the photo thermal energy of (Nd: YAG/second harmonic generation, 532 nm) that gained by the dopants which made it somewhat active, but at a lower rate compared with diodes b and c in Figure (4.2) mentioned previously.

All diodes in figure (4.6), exhibit a turn-on voltage of 0.7 V at 10 mA dc current. From this figure and table (4.3), the results show that the laser energy used is insufficient to induce activation of implanted impurities and also insufficient to reduce defects resulting from implantation of ions. Also figure (4.7) shows these results clearly where we found that the dynamic resistances are not changed significantly. This implies that the defects arising after the conventional annealing are still present.

4.4.3 Annealing by CW CO_2 laser (λ =10.6 μm), group III

From figure (4.8), the dynamic resistance of the diode before the laser treatment was calculated from the I-V characteristics curve to be 3.16 Ω. This figure shows two distinct regions: in the first region there is a clear decrease

in dynamic resistance up to 15 W of the input laser power, after which the dynamic resistance started to increase. In the first region, at the melt threshold value of input laser power, a substitution of impurity within the silicon lattice took place, resulting in an increase of electrical activity in the doped region. In the second region, when samples were treated with the laser power of 20, 25 and 30 W, the resistance values increased rapidly. This could be due to the diffusion of dopant and ablation effect. Due to the influence of an uncontrolled melting, an amorphous region in the substrate was resulted (I.A. Palani, N.J. Vasa, and M. Singaperumal et. al. 2010 , Raid A. Ismail and Aseel A. Hadi 2000).

The increase in the value of the dynamic resistance can be explained as follows: The incident laser power on silicon creates a large population of highly excited non-equilibrium electrons near the sample surface. This can lead to bond breaking, which is a thermal mechanism. Alternately, the excited electrons transfer energy to phonons during electron–phonon relaxation. The energy is redistributed through lattice vibrations and consequently heat is conducted into the sample. This heat may melt or vaporize the sample. Material removal in the form of large micrometer sized droplets can also resulted from hydrodynamic instability of the molten liquid layer (J. Lawrence, J. Pou, D. K. Y. Low 2010).

According to figure (4.9) and table (4.4), the diodes irradiated by 5, 10, and 15 watt, exhibit a turn-on voltage of 0.62, 0.61 and 0.597 V at 0.01 A. This could be attributed to the improvement in the surface structure and dopant activation.

4.4.3 Annealing by pulsed CO_2 laser (λ =10.6 μm), group IV

From figure (4.10) and table (4.5), one can see the deviation of the curve of the silicon diode before annealing from other curves due to the defects after furnace annealing. The diodes treated by energies of 500, 520, 540, 560, 580, and 600 mJ, respectively, exhibits forward voltage of 0.605, 0.6, 0.6, 0.595, 0.593, and 0.588 V at 10 mA.

The electrical conductivity of the silicon diodes changed as the laser energy increased from 500 to 600 mJ, because the carrier concentration is changed along with the increasing of laser energy. These results can be explained in terms of carrier trapping by the localized trap states at the grain boundary and the reduction of the trap state density with increasing laser energy. The trap state density also changed along with the number of laser pulses. By increasing the number of pulses, the trap state density can be reduced (Seiichiro Higashi, Kentaro Ozaki , Keiji Sakamoto et al. 1999).

Dynamic resistance of the silicon diodes in figure (4.11) decreased gradually from 3.16 to 2.56 Ω. This reduction can be explained as follows:

The grain size increased and the amorphous portion decreased, so that, less trapping states will exist in poly-Si films with big crystalline grains (Teixerira R.C., Doi I.; Zakia M. B. P. et. Al. 2002).This leads to a higher free carrier concentration, which reduces the resistivity and leading to decrease the dynamic resistance of the silicon diode.

Referring to figure (4.1), a large number of defects arising after furnace annealing due to incomplete atomic bonding exists in the grain boundaries, which forms trapping states. This reduces the number of free carriers available for electrical conduction. After trapping the mobile carriers, the traps become electrically charged and they create a potential barrier, which impedes the motion of carriers from one grain to another. The amorphous phase is also an insulating region, which implies in another potential barrier (Teixerira R.C., Doi I.; Zakia, M. B. P et. al. 2002). All these factors can affect negatively the behavior of I-V characteristics of silicon diode.

Laser annealing of Si has been demonstrated to offer advantages over furnace annealing such as exceeding the solid solubility limit of dopants in Si and having less defects after annealing, leading to the improvement in the electrical properties and hence the function of the junction subjected to ion implantation.

Most of the studies have been carried out on nanosecond laser pulses. This ns laser pulses provide fluences (energy densities) high enough to melt a surface layer of amorphous Si created by ion implantation of dopants on single crystalline silicon (D. V. Tran , Y. C. Lam, H. Y. Zheng et al. 2004). For both single crystalline Si (c-Si) and polycrystalline Si (poly-Si), the effect of dopant concentration on resistivity is essentially the same. Greater concentrations of carriers equate to lower resistance (Sidan Jin 2011).

4.5 Conclusions

The effect of laser annealing method to investigate the silicon diode was used and discussed. The obtained results showed that the defects arising after conventional annealing were decreased gradually after laser annealing, and the electrical properties such as I-V characteristics and dynamic resistance were improved after laser irradiation when they treated with energy of 1000 mJ and repetition rate of 3, 4, and 5 Hz by Q-switched Nd:YAG laser (λ=1064 nm). The results also showed a slight reduction of defects in the diode surface when the diodes were treated by the Q-switched Nd:YAG laser (λ=532 nm) with energy ranged from 300 to 450 mJ with different repetition rates.

CW CO_2 laser of power ranged between 5 to 15 W, reduces the voltage drop from 0.7 V for the diode before irradiation to 0.597 V after irradiation by 15 W, and the dynamic resistance also changed gradually from 3.16Ω to 2.6 Ω. When diodes treated with power of 20, 25, and 30 W, these powers increases the voltage drop across the diodes from 0.7 V to 0.72 V, and also increases the dynamic resistance of the diodes from 3.16 Ω to 3.48Ω. Single Pulse CO_2 laser also gives a good result for all diodes when irradiated 5 times by energies ranged between 500 to 600 mJ with constant pulse duration of 0.02 seconds. The results showed that the dynamic resistance reduced from 3.12Ω to 2.56Ω, and the voltage drop falls from 0.7 V before irradiation to 5.88 V after irradiation.

Annealing by CW and pulsed CO_2 with moderate power and energy introduced improvements in the electrical properties of diode such as I-V characteristics and dynamic resistance.

In conclusion, the infrared lasers such as Nd: YAG and CO_2 laser annealing is an important technique in the semiconductor industrial for improving the device performance. This result is potentially important to the improvement of semiconductor device's performance for both semiconductor industry and other possible research avenues.

4.6 Future work

For future work we suggest the followings:

1- Crystallization and annealing of amorphous-Si thin film by using third harmonics of Nd: YAG laser

2- Crystallization of amorphous Ge films by Excimer laser annealing

3- Formation of silicide by using Q- switched Nd: YAG laser.

4- Fabrication of Gap Capacitors.

References

1. Adelina Han and Dinu Gubencu (2008). Analysis of the laser marking. Nonconventional Technologies Review – no.4

2. Alberto Piqué , Bhanu Pratap, Scott A. Mathews et al. (2007). Laser Direct-Write of Embedded Electronic Components and Circuits. Materials Science and Technology Division, Naval Research Laboratory, Washington DC, USA.

3. Bo Lojek (2008). Low Temperature Microwave Annealing of S/D. 16th IEEE International Conference on Advanced Thermal Processing of Semiconductors – RTP Colorado Springs, CO 80906.

4. C. Charpentier, R. Boukhicha , P. Prod'homme et al. (2014). Evolution in morphological, optical, and electronic properties of ZnO:Al thin films undergoing a laser annealing and etching process. Solar Energy Materials & Solar Cells 125 (223-232).

5. Chen Wang, Cheng Li, Shihao Huang et al. (2014). Phosphorus diffusion in germanium following implantation and excimer laser annealing. Applied Surface Science 300 (208-212).

6. Chien-Yie Tsay and Tzu-Teng Huang (2014). Characterization of low-temperature solution-processed indium–zinc oxide semiconductor thin films by KrF excimer laser annealing. Ceramics International l40(8287–8292).

7. Chong Yung Fu (2003). Fabrication of Ultra-Shallow Junctions and Advanced Gate Stacks for ULSI Technologies Using Laser Thermal Processing. A thesis Submitted For The Degree of Doctor of Philosophy, Department of Electrical & Computer Engineering, National University of Singapore.

8. Colin E. Webb and Julian D.C. Jones (2004). Handbook of laser technology and applications. vol 1, Institute of physics, IOP publishing Ltd. UK.

9. Costas P. Grigoropoulos (2009). Transport in Laser Micro fabrication

Fundamentals and Applications. Cambridge University Press, UK.
10. D. E. Newbury, D. C. Joy, P. Echlin, et al. (1986). Advanced Scanning Electron Microscopy and X-Ray Microanalysis. Plenum Press. New York London ..
11. D. V. Tran , Y. C. Lam, H. Y. Zheng, et al. (2004). Femtosecond laser processing of crystalline silicon. published on Optics and Lasers in Engineering
12. G. Verma, S. Talwar and J. C. Bravman (2001). Creating process margin in laser thermal processing: Application to formation of titanium silicide. Appl. Phys. Lett. 78(7), 925.
13. Hammersley G., Hackel L.A., Harris F. (2000). Surface pre-stressing to improve fatigue strength by laser shot peening. J Optics Laser Eng 34, 327–337.
14. Harris J.and Brandt M. (2002). The cutting of thick steel plate using a spinning Nd:YAG laser beam. Industrial laser user 26 (24–25).
15. Hilton P.A., Jones I.A.,and Kennish Y. (2002) Transmission welding of plastics Proc Int Congress on Laser Advanced Material processing (LAMP 2002) pp (1–13).
16. I.A. Palani, N.J. Vasa, and M. Singaperumal, et al (2010). Investigation on Laser-annealing and Subsequent Laser-nanotexturing of Amorphous Silicon (a-Si) Films for Photovoltaic Application. JLMN-Journal of Laser Micro/Nanoengineering Vol. 5, No. 2.

17. J. K. Sheu, J. M. Tsai, S. C. Shei, W. C. Lai, T. C. Wen, C. H. Kou, Y. K. Su, S. J. Chang, and G. C. Chi (2001). Low-Operation Voltage of InGaN/GaN Light-Emitting Diodes With Si Doped $In0_{:3}Ga_{0:7}N$/GaN Short-Period Superlattice Tunneling Contact Layer. IEEE Electron device letters, VOL. 22, NO. 10, OCTOBER 2001
18. J. Lawrence, J. Pou, D. K. Y. Low and E. Toyserkani (2010). Advances in laser materials processing. Woodhead Publishing Limited.
19. J. Powell and A. Kaplan (2004). Laser Cutting: From First Principles to

the state of the art. Proceedings of the 1st Pacific International Conference on Application of Lasers and Optics.

20. J.S. Luo, W.T. Lin, C. Y. Chang et al (2000). Instrum. Methods. Phys. Res. Sect. B, 169, 124.

21. John C. Ion et al. (2005). Laser Processing of Engineering Materials. UK: Elsevier.

22. John F.Ready (1997). Industrial applications of lasers. Second edition, San Diego, Academic Press.

23. K. Thyagarjan and Ajoy Ghatak (2010). Lasers Fundamentals and Applications. Springer Science+Business Media, LLC 1981.

24. Lee J.M. (2002). Advanced laser cleaning techniques in Lee J.M. Lasers and cleaning process Hanrimwon, Korea ISBN89-85670-87-5.

25. Leonard Rubin and John Poate (2003). Ion Implantation in Silicon Technology. American Institute of Physics.

26. M. C. Li, X.K. Chen, W. Cai et al. (2001). Mater. Chem. Phys. 72, 85.

27. M. Rahimo, J. Vobecký, C. Corvasce and Y. Otani (2012) Thin Silicon Wafer Device Concept with Advanced Laser Annealing and Sintering Process. IEEE. Reprinted from the Internacional Seminar on Power Semiconductors.

28. Mark Goorsky (2012). Ion Implantation. Rijeka, Croatia : InTech

29. Matthew Werner (2006). Damage formation and annealing studies of low energy ion implants in silicon using medium energy ion scattering. Submitted in partial fulfillment of the requirements of the degree of Doctor of Philosophy, The University of Salford, UK.

30. Mazumder J., Dutta D., Kikuchi N.et al. (2000). Closed loop direct metal deposition: art to part. J. Optics and Lasers Eng. 34, (397–414).

31. Miin-Horng Juang, C.N. Lu , S.L. Jang et al.(2010). Study of ultra-shallow p+n junctions formed by excimer laser annealing. Materials Chemistry and Physics (123) 260–263

32. Min Gyu Kang, Kwang Hwan Cho, Seung Min Oh, et. al. (2011). Low-

temperature crystallization and electrical properties of BST thin films using excimer laser annealing. Current Applied Physics 11(S66-S69).
33. Peter Schaaf (2010). Laser Processing of Materials. Fundamentals, Applications, and Developments. Springer Series in Materials Science. 34. Phillip Sandborn and Peter A. Sandborn (2008). A Random Trimming Approach for Obtaining High-Precision Embedded Resistors. IEEE Trans. On Advance Packaging, Vol. 31, No. 1, pp. (76-83).
35. Raid A. ISMAIL, Aseel A. HADI (2000). Electrical Characteristics of Si Doped with Sb by Laser Annealing. Department of Applied Sciences, University of Technology Baghdad-IRAQ.
36. Romain Beal, Khalid Moumanis, Vincent Aimez et al. (2013). Enhanced spectrum superluminescent diodes fabricated by infrared laser rapid thermal annealing. Optics & Laser Technology 54 (401-406).
37. S.A. Moshkalev V.A. Ermakov , A.R. Vaz et al. (2014). Formation of reliable electrical and thermal contacts between grapheme and metal electrodes by laser annealing. Journal of Microelectronic Engineering 121 (55-58).
38. S.Y. Chen, Z. X. Shen, and S. Y. Xu et al. (2002). Electrochem Soc. 149, G609.
39. Seiichiro Higashi, Kentaro Ozaki , and Keiji Sakamoto et al (1999). Electrical Properties of Excimer-Laser-Crystallized Lightly Doped Polycrystalline Silicon Films. Jpn. J. Appl. Phys. Vol. 38 (857–860).

40. Shailesh siddha and Yashika Chander Pareek (2013). Fabrication of PN-Junction Diode by IC Fabrication Process. International Journal of Innovative Research in Science, Engineering and Technology Vol. 2, Issue 10, ISSN: 2319-8753
41. Sidan Jin (2011). Boron Activation and Diffusion in Polycrystalline Silicon with Flash- Assist Rapid Thermal Annealing. A dissertation presented to the graduate school of the university of Florida in partial fulfillment of the required for the degree of Doctor of Philosophy,

university of Florida.

42. Silve S. Laser forming and creative metal work (2000). PhD Thesis Buckinghamshire Chilterns University and Brunel University.

43. Taj Muhammad Khan, M. Zakria, Mushtaq Ahmad et al (2014). Optoelectronic study and annealing stability of room temperature pulsed laser ablated ZnSe polycrystalline thin films. Journal of Luminescence 147 (97-106).

44. Teixerira R.C., DOI I.1; ZAKIA, M. B. P. et. al.(2002). Grain Size Influence on Sheet Resistance of P- and AS-Implanted Polycrystalline Silicon Deposited by Vertical CVD Reactor. Center for Semiconductors Components – State University of Campinas, R. Pandiá Calógeras, 90, CEP: 13083-970, Caixa Postal 6061, Campinas – SP – Brasil

45. W. W. Du'ley (1983). Laser Processing and Analysis of Materials. Plenum Press, New York.

46. W.W. Duley (2005). UV lasers: effects and applications in materials science . Cambridge University Press.

47. Weilie Zhou and Zhong Ling Wang (2006). Scanning Microscopy for Nanotechnology Techniques and Applications. Springer

48. William M. Steen,, Jyotirmoy Mazumder (2010). Laser Material Processing. springer, 2010.

49. Y.F. Chong, K. L. Pey, A. T. S. Wee, et al. (2001). Electron. Mater. 30, 1549

50. Yanmin Guo , Liping Zhu, Jie Jiang et al. (2014). Enhanced performance of NiMgO-based ultraviolet photodetector by rapid thermal annealing. Thin solid Films (558) 311 -314.

51. Zhanyong Wang, Hongyang Zhao, Qiwen Yao et al (2013). The influence of layer thickness and post annealing on magnetism of pulsed laser deposited ZnO/Co multilayers. Journal of Magnetism and Magnetic Material (345) p 41-47.